Chemical Engineering Journal 331 (2018) 870–894

Contents lists available at ScienceDirect

Chemical Engineering Journal

journal homepage: www.elsevier.com/locate/cej

Optimization of the design, operating conditions, and coupling configuration of combined cycle power plants and CO_2 capture processes by minimizing the mitigation cost

Patricia L. Mores[a,1], Juan I. Manassaldi[a,1], Nicolás J. Scenna[a], José A. Caballero[b], Miguel C. Mussati[a,c], Sergio F. Mussati[a,c,*]

[a] CAIMI Centro de Aplicaciones Informáticas y Modelado en Ingeniería, Universidad Tecnológica, Nacional, Facultad Regional Rosario, Zeballos 1346, S2000BQA Rosario, Argentina
[b] Department of Chemical Engineering, University of Alicante, Apartado de correos 99, 03080 Alicante, Spain
[c] INGAR Instituto de Desarrollo y Diseño (CONICET-UTN), Avellaneda 3657, S3002GJC Santa Fe, Argentina

ARTICLE INFO

Keywords:
Natural gas combined cycle NGCC
Post-combustion CO_2 capture
Mitigation cost
Optimal coupling schemes
NLP model
GAMS

ABSTRACT

This paper deals with the optimization of the coupling between a natural gas combined cycle (NGCC) plant and a post-combustion CO_2 capture process by minimizing the mitigation cost – defined as the ratio between the cost of electric power generation and the amount of CO_2 emitted per unit of total net electric power generated – while satisfying the design specifications: electric power generation capacity and CO_2 capture level. Three candidate coupling configurations, which differ in the place where the steam is extracted from, are optimized using detailed and rigorous models for both the NGCC and the CO_2 capture plants. By comparing the mitigation cost of each configuration, the optimal integration configuration and the corresponding optimal sizes and operating conditions of all process units (steam turbines, gas turbines, heat recovery steam generators HRSGs, absorption and regeneration columns, reboilers and condensers, and pumps) are provided. In the computed optimal solution, the steam required by the CO_2 capture plant is extracted from both the steam turbine and the HRSG (evaporator operating at low pressure), and the mitigation cost is 90.88 \$/t CO_2. The optimal solution is compared with suboptimal solutions corresponding to the other two candidate coupling schemes. These solutions are compared in detail regarding capital investment and operating costs, HRSG configuration, process unit sizes, and operating conditions.

1. Introduction

The combustion of fossil fuels for electricity generation, industry, and transportation is the largest source of CO_2 emissions, and it is considered to be the main contributor to the greenhouse effect. The reduction of CO_2 emissions is one of the most challenging issues that the world community faces today, which requires joint actions and close cooperation between government, industries, and researchers.

The most important strategies to reduce the global CO_2 emissions are the CO_2 capture and storage (CCS) and the CO_2 capture and utilization (CCU), which differ in the final destination of the captured CO_2. In the former the captured CO_2 is transferred to a suitable site for long-term storage whereas in the latter the captured CO_2 is converted into valuable fuels, chemicals, building materials, and other products. Cuéllar-Franca and Azapagic [1] and Kravanja et al. [2] presented an overview of recent advances in CCS and CCU, among other environmental issues.

There are studies in which the CO_2 is utilized as a carbon source for methanol production [3–6]. Roh et al. [6] developed a methodology for a sustainable design and implementation strategy of CO_2 utilization processes. They considered two CO_2 utilization processes for methanol production: combined reforming and direct synthesis. They showed that the integration or replacement of an existing conventional methanol plant with a combined reforming process represents a sustainable solution. Furthermore, there are studies in which the CO_2 is utilized for the production of dimethyl carbonate [7], dimethyl ether [8], urea [9], and for enhanced oil recovery (EOR) [10]. Kongpanna et al. [7] applied a systematic computer-aided framework for the synthesis and generation of processing networks for dimethyl carbonate production with CO_2 utilization. Martin [8] proposed a mathematical

* Corresponding author at: INGAR Instituto de Desarrollo y Diseño (CONICET-UTN), Avellaneda 3657, S3002GJC Santa Fe, Argentina.
E-mail address: mussati@santafe-conicet.gov.ar (S.F. Mussati).
[1] Contributed equally to this article.

http://dx.doi.org/10.1016/j.cej.2017.08.111
Received 6 June 2017; Received in revised form 21 August 2017; Accepted 22 August 2017
Available online 24 August 2017
1385-8947/

Nomenclature

Symbols

AC	total additional cost (M$/yr.)
CAPEX	capital expenditures (M$)
COE	cost of electric power generation ($/MWh)
CRF	capital recovery factor (dimensionless)
C_{inv}	total investment cost (M$)
C_{inv}^{k}	individual acquisition cost of the pieces of equipment (k) of the power plant and the capture system (M$)
C_{mant}	cost of maintenance (M$/yr.)
C_{mp}	cost of manpower (M$/yr.)
C_{rm}	cost of raw materials and utilities (M$/yr.)
C_{rm}^{u}	specific cost of raw materials and utilities ($/t, $/GW)
C_S	supervision and support labor (M$/yr.)
DMC	total direct manufacturing cost (M$)
E	amount of CO_2 emitted per unit of total net electric power generated (kg/MWh)
f_1, f_2, f_3	economic indexes (dimensionless)
g_t	set of inequality constraints t
HETP	height equivalent to a theoretical plate (m)
HTA	heat transfer area (dam^2)
HTU	height of a transfer unit (dimensionless)
h_s	set of equality constraints s
i	interest rate (%)
IFC	investment on fix capital (M$)
IMC	total indirect manufacturing cost (M$)
LMTD	logarithm mean temperature difference (K)
MC	minimal mitigation cost ($/t CO_2)
m^u	annual consumption of raw materials and utilities (kg/yr.)
MW_{CO2}	molecular weight of CO_2 (g/mol)
MW^{34}	molecular weight of gaseous mixture in the stream #34 (g/mol)
OPEX	operating expenditures (M$/yr.)
PC	total production cost (M$/yr.)
R_{CO2}	CO_2 recovery (%)
TAC	total annual cost (M$/yr.)
W_{GT}	net electric power generated by the gas turbines (MW)
W_{net}	required total net electric power generation (MW)
W_{ST}	net electric power generated by the steam turbines (MW)
W_B^{CP}	total electric power required by blowers B in the CO_2 capture plant CP (MW)
W_C^{PP}	total electric power consumed by compressors C in the NGCC power plant PP (MW)
W_C^{CP}	total electric power required by compressors C in the CO_2 capture plant CP (MW)
W_P^{PP}	total electric power consumed by pumps P in the NGCC power plant PP (MW)
W_P^{CP}	total electric power required by pumps P in the CO_2 capture plant CP (MW)
W_{net}	generated total net electric power (MW)
NTU	number of transfer units (dimensionless)
N_{CT}	number of CO_2 capture trains (dimensionless)
N_{GT}	number of gas turbines (dimensionless)
N_P	number of pumps (dimensionless)
N_{ST}	number of steam turbines (dimensionless)
n	project lifespan (yr.)
X^k	size of the process unit k (dam^2, MW, m^3)

Acronyms

CCS	CO_2 capture and storage
GAMS	General Algebraic Modeling System
HETP	height equivalent to a theoretical plate
HRSG	heat recovery steam generators
HTA	heat transfer area
HTU	height of a transfer unit
IGCCs	integrated gasification combined cycles
LMTD	logarithm mean temperature difference
MINLP	mixed-integer nonlinear programming
NGCC	natural gas combined cycle
NLP	nonlinear programming
NTU	number of transfer units
SNG	synthetic natural gas

Abbreviations

AE, IC, CT	heat exchangers
AMP	amino-methyl-propanol
B	blower
BZA	benzylamine
C	condenser
CC	combustion chamber
COM	compressors
C1, C2, C3	coupling scheme
EC	economizer
EC	lean/rich solutions cross heat exchanger
EV	evaporator
EX	expander
GEN1, GEN2	generator
GT	gas turbine
gPROMS	general PROcess Modelling System
HMPD	4-hydroxy-1-methylpiperidine
HPST	high pressure steam turbine
IPST	intermediate pressure steam turbine
LPST	low pressure steam turbine
MEA	monoethanolamine
OS	optimal solution
P, CO_2P	pumps
P1	optimization problem
PZ	piperazine
R	reboiler
REG	regeneration column
SH	superheater
SOS1, SOS2	suboptimal solution

Subscript

PP + CP	NGCC power plant coupled to the CO_2 capture plant
SAPP	NGCC power plant operating in a standalone mode

Greek letters

α_{CO2}	CO_2 loading in the liquid phase (mol/mol)
τ	working hours per year (8000 h/yr.)

optimization framework to select the flow sheet and determine the operating conditions for the synthesis of dimethyl ether from CO_2 captured and H_2 produced by water electrolysis using renewable energy sources such as solar or wind energy. Hasan et al. [10] developed a multi-scale framework for CO_2 capture, utilization, and storage (CCUS) to minimize costs while reducing the stationary CO_2 emission in USA. The studies have shown that more than 3% of the total stationary CO_2 emission in USA can be eliminated by a CCUS network. Bose et al. [9] investigated the possibility of recycling the CO_2 captured at coal-based power plants rather than its capture and storage which would

require a large amount of energy. In particular, they proposed a solution where the captured CO_2 would be used for urea production. An overview about computational methods and tools as a complement to experiments as well as advantages and disadvantages of the available technologies for CO_2 capture and conversion, ideas and perspectives for the development of new techniques, opportunities, and challenges can be found in Yuan et al. [11].

The chemical CO_2 absorption using amines is considered to be the most mature post-combustion technology for CO_2 capture to be implemented in the midterm for both existing and new power plants. The first commercial amine-based CO_2 capture installation started operating in 1996 in Norway in response to carbon taxes. Since then, the firm Statoil has captured from the Sleipner West gas field – and stored – into an aquifer beneath the North Sea around 1 Mt of CO_2 per year [12]. Dow Chemical Co. (later Fluor Daniel Inc.), Kerr-McGee Chemical Corp., and ABB Lummus Crest Inc. were among the initial developers of the amine-based CO_2 capture technology [12]. Today, there are 17 large-scale CCS installations in operation and 4 in construction that can remove around 37 Mt of CO_2 per year, encompassing a wide range of CO_2 capture technologies. In addition, there are 7 projects in advanced development stage and 11 projects in early development stage [13]. The variety of industries using large-scale CCS installations (power, steel-making, natural gas processing, fertilizers, plastics, chemicals, and hydrogen for refining, among others) shows the flexibility of the CCS technology. A list with all the large-scale CCS installations with their lifecycle stage, location, industry, capture type and capacity, and primary storage type can be found in [13], and some pilot-scale demonstrations of CO_2 capture from power plants by means of chemical absorption using amines can be found in [14–17]. However, this process is considered to be an intensive energy process because of the high requirement of thermal energy to regenerate the amine, which leads to a significant reduction in the electricity generation in the power plant and constitutes a major challenge of this alternative. In addition, the low CO_2 concentration level in the flue gas streams is another important technical issue that poses another challenge to research. Because of the fact that the natural gas combined cycle (NGCC) plants and CO_2 capture processes are strongly coupled they should not be designed as stand-alone processes [18]. For this reason, a great research effort is being mainly focused on reducing the amine regeneration energy by improving the absorption process, and on determining how the power plants and the capture processes should be integrated in order to efficiently use the steam generated in the power plants.

Several research groups are exploring the potential of new solvents with the aim of achieving better overall properties for applications in CO_2 capture [19–25]. Richner et al. [19] investigated the CO_2 absorption into aqueous solutions of benzylamine (BZA) as well as formulations of BZA/monoethanolamine (MEA) and BZA/amino-methyl-propanol (AMP). The results showed that the CO_2 mass transfer coefficients obtained for BZA formulations are larger than the ones obtained for unblended MEA. Fu et al. [20] experimentally investigated in a lab-scale absorber the performance of CO_2 absorption into a hybrid solvent such as MEA in methanol (MeOH). They observed that the overall gas phase mass transfer coefficient for MEA–MeOH was higher than that for MEA–H_2O. Experimental research conducted by Du et al. [21] showed that aqueous solutions of piperazine (PZ)/4-hydroxy-1-methylpiperidine (HMPD) exhibit a much greater solvent stability than MEA as well as lower volatility for CO_2 capture from flue gases. However, other authors argued that (i) MEA is the most applicable amine especially for low CO_2 partial pressures in the flue gas [26], (ii) MEA is the cheapest of the important liquid absorbents [27], (iv) MEA is recognized as a first choice or the benchmark solvent for power plants due to the fast CO_2 absorption rate [28], and (v) MEA is the most efficient amine for CO_2 absorption, with efficiency values over 90% [29].

Experimental works are indispensable to accurately identify promising mixtures for CO_2 capture. However, it is a challenging task due to increased combinatorial complexity and the non-ideal chemical interactions, requiring to consider multiple selection criteria. This results in experimental costs and effort that become prohibitive for the investigation of a large number of mixtures. In this sense, the use of computer-aided tools can help address these challenges through models that enable accurate predictions of the desired mixture properties and systematic procedures to account for the combinatorial complexity [30]. In fact, several research groups have evaluated the design of mixtures for CO_2 capture through computer-aided molecular design (CAMD) approaches [31–38]. Burger et al. [32] proposed a hierarchical methodology based on a group contribution method which considers the molecular decisions at the same level of the process design decisions. They applied their method for selecting the optimal solvent over a wide range of ethers for CO_2 separation from a methane rich mixture. Bommareddy et al. [31] formulated an alternative optimization problem in which the aim is to find the optimal physical properties that minimize the process costs without considering the solvent chemical structure explicitly. Once the optimal values of the properties have been identified, the chemical structures (pure components and mixtures) that possess these properties are found by solving a separate CAMD problem. Chong et al. [34] developed a CAMD approach for selecting optimal ionic liquids (ILs) for CO_2 capture from combustion flue gases. Group contribution methods were used to estimate the physical and thermodynamic properties of ILs by considering the structural constraints and allowing the combination of cations and anions. Papadopoulos et al. [35] presented an approach for the screening and selection of post-combustion CO_2 capture solvents based on the performance criteria of several thermodynamics, reactivity, and sustainability properties. Porcheron et al. [36] developed a statistical, neural network model for fast prediction of the pseudo-acidity constant and the absorption isotherms for amines used in CO_2 capture, providing evidence that simple models may facilitate a quick and reliable screening of CO_2 capture solvents prior to utilizing rigorous models or lab-scale experiments. Venkatramana et al. [38] proposed an efficient evolutionary approach to find promising absorbents for CO_2 capture by optimization of the acid dissociation constant (pKa). They introduced a systematic computational study in which a genetic algorithm was used for the generation and screening of novel imidazole-based agents. They identified promising absorbents with high values of dissociation constant.

Other researchers are investigating alternative methods for solvent regeneration, such as methods based on electrochemistry, photochemical processes, or electromagnetic radiation [39–41].

The application of mathematical modeling, simulation, and optimization of decoupled power plants, decoupled CO_2 capture plants, and power plants coupled to CO_2 capture plants is another research area which has been receiving particular attention during the last years.

Indeed, there have been published several articles dealing with the study of *stand-alone* power plants [42–48]. Martelli et al. [43] proposed and implemented an automatic methodology to simultaneously optimize the design of simple combined cycles. The sizes of heat recovery steam generators (HRSGs), mass flow rates, pressures, and temperatures of all the streams (steam/water), as well as the mass flow rates of fuel used for supplementary firing, were considered as optimization variables. They successfully applied the proposed model and methodology to highly integrated plants such as biomass to Fischer-Tropsch liquid plants, integrated gasification combined cycles (IGCCs) with and without CCS, and coal to synthetic natural gas (SNG) facilities. Wang et al. [44] combined mixed-integer nonlinear programming (MINLP) and multi-objective techniques for analyzing the parametric and structural optimization of supercritical coal-fired power plants to investigate the economically-optimal designs at different efficiency levels. They proposed a superstructure-based model that embeds up to ten feedwater preheaters, up to two reheaters, and a secondary turbine with steam extractions. Zhang et al. [46] recently developed a superstructure based on a MINLP model for the design optimization of a HRSG considering different alternative layouts of HRSG and connections between the HRSG and other external heat exchangers, using coal as fuel. The

model is solved to determine the optimal arrangement for several case studies involving two and three pressure levels with and without steam reheating. Manassaldi et al. [47] developed a MINLP model for the optimal synthesis and design of dual pressure HRSGs coupled into two steam turbines which allowed to obtain a more efficient configuration compared to the configuration obtained by Zhang et al. [46] because of the fact that the proposed superstructure embedded more alternative configurations. Also, there are articles dealing with the study of combined cycles using biogas [49–52]. León and Martín [51] formulated a nonlinear mathematical programming (NLP) model to optimize combined cycle power plants firing biogas obtained by anaerobic digestion of a mixture of cattle and pig slurry. The model, which was implemented in the GAMS environment, allows to simultaneously obtain the optimal operating conditions and the best process configuration to efficiently generate steam from the flue gas. They evaluated two alternative configurations differing in the flow pattern of the flue gas. Kang et al. [49] addressed the study of natural gas and biogas co-firing in gas turbine combined heat and power systems. They performed simulations in the GateCycle Software [53] to analyze the influence of the input ratios of natural gas and biogas and heat sale ratio on the cost of electricity (COE), payback period, and net present value, among others. Yağlı et al. [52] designed organic Rankine cycles (ORC), recovering waste heat from a combined heat and power (CHP) engine harnessing biogas produced from domestic wastes. They studied and compared two ORCs: subcritical and supercritical. The comparison indicated that the supercritical ORC has better performance in terms of cycle net power, thermal efficiency and exergy efficiency. Developments of biogas combustion in CHP generation are reviewed in Hosseini and Wahid [54].

Regarding CO_2 capture processes, there have been also published several articles dealing with the mathematical modeling, simulation, and optimization of *stand-alone* CO_2 capture processes using amines. Some authors have employed commercial process simulators such as ASPEN [55–59], HYSYS [60], and ProMax [61]. For instance, by using ASPEN, Zhang et al. [55] identified the reactions that significantly affect the regeneration of aqueous ammonia. To this end, they performed a simulation study varying the main operating conditions (temperature, pressure, CO_2 loading, among others). They provided a useful guidance to reduce the energy required for the amine regeneration. Lin and Rochelle [57] applied an exergy analysis to investigate the contribution of each piece of equipment to the total inefficiency of the regeneration process. As in Zhang et al. [55], they carried out parametric simulations using ASPEN to perform a reaction sensitivity analysis of the regeneration process of CO_2 capture using aqueous ammonia for several regenerator configurations. Rodriguez et al. [60] employed HYSYS to minimize the total annual cost of a complete CO_2 capture process using equilibrium stage models for both the absorption and regeneration processes and a detailed cost model. The effect of the main process variables on the total cost was analyzed in detail considering three alkanolamine solutions (diethanolamine MDEA, MEA, and MDEA-MEA solution). To treat a gas flow rate of 2.8 10^{-4} kgmol/h at 200 °C with 4% CO_2 targeting a CO_2 capture level of 80%, the minimal total cost (2.146 $/t CO_2) was computed for a solution containing 20% MDEA and 20% DEA in water (wet weight). Liang et al. [61] presented a review of different methods – from empirical design methods to pilot plant techniques – that can be employed for the design of CO_2 absorption columns focusing on the column dimensions (diameter and height). They used the software ProMax to simulate four existing pilot plants located in Canada (International Test Centre of CO_2 Capture pilot plant), Denmark (Esbjerg CASTOR pilot plant), Germany (Institute of Thermodynamics and Thermal Process Engineering), and Norway (SINTEF/NTNU pilot plant). Other research groups have employed equation-oriented environments such as MATLAB [62,63], COMSOL [64], and gPROMS [65–75]. Lawal et al. [65] developed in gPROMS two dynamic models of the absorption column for post-combustion CO_2 capture with MEA: an equilibrium-based model and a rate-based model to study the dynamic behavior of the absorber during part load operation and with changes from the regenerator. One of the analyzed scenarios has been to study the effect of disturbances of lean MEA solution loading in the performance of the absorber. They showed that the CO_2 absorption recovery drops almost 10% (from 94% to 85%) when the CO_2 loading in the lean solution increased from 0.28 to 0.307. Also, they found that the increase in the flow rate of the solvent (lean MEA) or the decrease in the CO_2 loading CO_2 absorption levels can keep high CO_2 capture levels. Harun et al. [70] developed in gPROMS a dynamic rate-based model of the CO_2 capture absorption process considering MEA as solvent to predict the dynamic behavior. The predicted results were validated with results obtained from steady-state simulations performed in Aspen and data reported in the literature. Mac Dowel and Shah [68] implemented in gPROMS a mathematical model of a coal-fired power plant coupled with a MEA-based CO_2 capture process with the aim of studying the dynamic operation. They proposed a simple modification to the amine-regeneration process to reduce the energy requirement in the reboiler, which consists of splitting the lean amine stream after the rich-lean heat exchanger into two streams; both of them exchange heat with cooling water but one is fed at the top of the absorber and the other one in the middle. Alhajaj et al. [67] developed in gPROMS an optimization mathematical model of a CO_2 capture plant and compression train to minimize the total cost for different CO_2 capture levels. The amine lean loading and the reboiler and regenerator pressures were considered as the control variables and the absorber height and diameter as the main design variables, which were simultaneously optimized. They discussed the contribution of the different process units to the total capital and operation expenditures. Luu et al. [75] implemented in gPROMS a mechanistic rate-based model to study and compare a standard proportional–integral–derivative (PID) feedback control scheme, a cascade PID scheme, and a model predictive control (MPC) based control structure for stepwise set-point tracking and load change scenarios for CO_2 capture facilities. The MPC strategy performs better than PID based control schemes, and it is capable of keeping the system at the target set-points while meeting operating, economic, and environmental criteria. Other authors have developed in-house simulation algorithms [76,77]. Only a few articles have been found in the literature dealing with the simultaneous optimization of the process unit sizes (design) and operating conditions of the entire post-combustion CO_2 capture process – absorption, amine regeneration, and compression stages – based on detailed cost equations and rigorous mathematical modeling of the process units [67,78–83]. Mores et al. [78] implemented in GAMS an equilibrium-based model for the CO_2 absorption column using “the height equivalent to a theoretical plate concept” (HETP) to compute the packed height of the column. After model verification using experimental data reported in literature, the proposed model was employed to determine the optimal operating conditions that lead to the maximum absorption efficiency defined as the ratio between the CO_2 recovery and the packing volume of the column considering both the column height and diameter as optimization variables. The effect of the main process parameters was also investigated. Mores et al. [79] developed a detailed model of the entire CO_2 capture plant (absorption and regeneration processes) including the compression stages and proposing a detailed cost model. They performed several optimizations to simultaneously find the optimal design and operating conditions that minimize the total annual cost while meeting different CO_2 reduction targets.

Regarding the *coupled* combined cycle power plants with post-combustion CO_2 capture plants, there exist several studies dealing with the dynamic operation of these facilities. [73,84–88]. Adams and Mac Dowell [84] have implemented in gPROMS a detailed mathematical model of a 420 MW reheat combined cycle gas turbine (CCGT) plant operating with three pressure levels to evaluate the technical and economic performances under full and part load conditions. The model output results were compared to the ones predicted by an equivalent model implemented in Thermoflow THERMOFLEX [89] in terms of

power output and efficiency. The developed model was then integrated with a dynamic model of an MEA-based CO_2 capture process implemented also in gPROMS. They concluded that CCGT power plants coupled to CO_2 capture processes are well suited to dynamic operation. Ali et al. [85] modeled in Aspen Plus different 800 MW_e power generation systems coupled to a MEA-based CO_2 capture plant and a CO_2 compression unit. They showed that standalone NGCC and integrated NGCC with CO_2 capture and CO_2 compression systems result in net efficiency values higher than the pulverized supercritical coal and biomass fired power plants, and with the least CO_2 emissions. However, the least efficiency penalty due to the integration of the power plant with CO_2 capture and compression systems was observed for the NGCC operating with exhaust gas recirculation (EGR). In addition, comparatively higher efficiency penalty and higher specific CO_2 emissions were observed for biomass fired power plants. Montañés et al. [86] studied the dynamic interactions between a NGCC power plant and a CO_2 capture plant using MEA during load change transient operation employing detailed and linked dynamic models. They considered control structures for both the steam cycle and the post combustion unit, and concluded that coupling a CO_2 capture plant to a NGCC does not significantly affect the load-following capability of the integrated system highlighting the need of having a suitable control structure for steady-state and transient conditions. They identified the liquid-to-gas ratio of the absorbers as the control variable that leads to faster stabilization times of the main process variables of the entire facility.

Also, there have been published papers addressing the simulation of coupled power plants with CO_2 capture plants dealing with steady-state operation; many of them dealt with simulation and simulation-based optimization for the retrofit of CO_2 capture processes to existing power plants considering several scenarios [90–99]. Dave et al. [90] studied the efficiency of existing and new coal-fired power plants for different CO_2 capture levels and cooling options. Li and Liang [97] investigated the retrofit of an ultra-supercritical pulverized coal-fired power plant located in China (Shandong province) with a capacity of 1000 MW. The study was conducted considering technical and economic aspects. They highlighted that the value of retrofitting option is significant and concluded that the economic feasibility of retrofitting to CO_2 capture is sensitive to the carbon price development and regulatory requirements during the plant lifetime. However, only few articles can be found in the literature focusing on the *simultaneous* optimization of the process unit sizes, and operating conditions of integrated CO_2 capture-NGCC plants, based on gradient [100–103] or meta-heuristic optimization methods such as genetic algorithms and simulated annealing algorithms [104–106]. Some authors employed a superstructure-based optimization approach for coupled power and CO_2 capture plants [59,102,107–112]. Lee et al. [59] recently proposed a superstructure-based methodology for the optimal retrofit of a CO_2 capture pilot plant located in South Korea using a rigorous rate-based model for the reactive distillation. Solvent recirculation and multiple vapor recompression processes (lean and rich vapor recompression) were embedded in the superstructure among the candidate configurations for the amine regeneration section. The rigorous model was implemented in Aspen Plus and the optimization of the superstructure was carried out using a genetic algorithm, for which the authors developed a Matlab-Aspen Plus interface. The results indicated that the optimal retrofit process includes solvent recirculation in three stages, lean vapor recompression, and mechanical vapor recompression, which allowed to reduce the thermal energy and total energy consumption by around 59% and 27%, respectively. Cristobal et al. [107] proposed a systematic tool and a bi-criteria MINLP model to assist in selecting optimal retrofit options in coal-fired power plants, including CO_2 capture technologies (chemical absorption with MEA and oxy-fuel combustion). They found that CO_2 capture with MEA performs better for soft limits, while oxy-fuel combustion is preferred when more stringent environmental limits are imposed. Manassaldi et al. [102] proposed a superstructure-based NLP model, which was implemented in GAMS, aiming at simultaneously determining how to optimally integrate the NGCC plant and the CO_2 capture process in order to maximize the overall efficiency and computing the corresponding optimal operating conditions and sizes of the process units. The overall efficiency was defined as the ratio between the total net electricity generated and the fuel consumed. They concluded that the final integrated process configuration, design, and operating conditions should be made in terms of the total investment and operating costs.

In this context, the main aim of this paper is to address the optimization of the integration of NGCC plants and the CO_2 capture process by absorption with MEA that minimizes the mitigation cost – also referred to as the CO_2 avoided cost. More precisely, the main objective is to examine the coupling schemes previously studied by Manassaldi et al. [102] but using an economic criterion (minimization of the mitigation cost) instead of an energetic criterion (maximization of the overall efficiency). To this end, detailed cost models for both the power plant and the CO_2 capture plant were included to compute the mitigation cost. As discussed above, to the best of our knowledge, there is not much previous work that exploits the benefit of rigorous optimization approaches to simultaneously optimize the NGCC plant and the post-combustion CO_2 capture process, process unit sizes, and operating conditions.

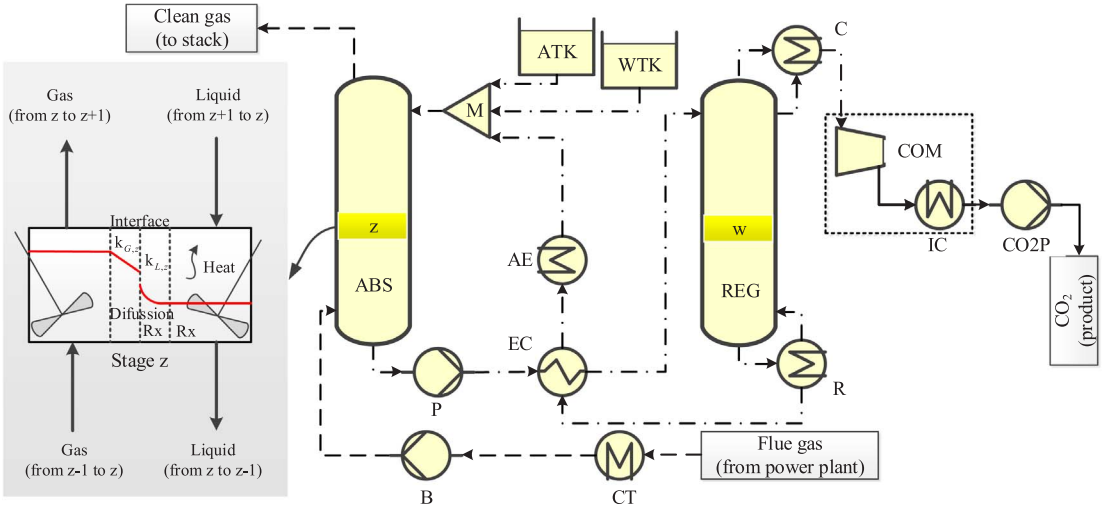

Fig. 1. Schematic of a chemical CO_2 capture plant.

2. Process description

2.1. CO_2 capture plant

Fig. 1 shows that the main pieces of equipment required in the CO_2 capture process are the absorber ABS, the amine regeneration column REG involving a reboiler R and a condenser C, the lean/rich solutions cross heat exchanger EC, compressors COM, pumps P and CO_2P, a blower B, and heat exchangers AE, IC, and CT. The exhaust gases leaving the HRSG are delivered into the bottom of the packed absorber and flows upward to contact the lean amine stream that comes from the regenerator unit and enters at the top of the absorber. The rich amine carrying the acid gases leaves the bottom of the absorber, passes first through the lean/rich solutions heat exchanger and then through the filter to remove solid impurities. Afterward, the rich solution flows downward through the regeneration column. Acid gases are removed from the stream and the condensed steam returns to the regenerator as reflux. Usually, the steam required by the reboiler is generated in the power plant influencing its thermal efficiency because the electricity generation capacity is reduced. Purified amine leaves the regenerator and goes through the amine–amine heat exchanger and solution cooler before returning to the absorber. The volume of recovered CO_2 strongly influences the number and capacity of the compressors.

The CO_2 loading factor, defined as the ratio between the total moles of CO_2 and the total moles of amine in the liquid phase, is a key parameter for CO_2 capture utilizing amines, which depends on the amine type. The reboiler heat duty of the regenerator unit is strongly influenced by the amine type and composition. Because of the strong relationships established among all the process variables, they should be simultaneously considered when analyzing the entire process, i.e. the CO_2 capture plant coupled to the power plant.

2.2. Natural gas combined cycle (NGCC) power plant

Fig. 2 shows a basic scheme of a NGCC power plant, which consists of a gas turbine GT including a compressor COM, a combustion chamber CC, and a expander EX coupled to a generator GEN1; a heat recovery steam generator HRSG; and steam turbines HP, IP and/or LP ST coupled to a generator GEN2. The gas turbine GT operates on the principle of the Brayton cycle, where air is first compressed in COM and then combusted with natural gas in CC; the combustion gases are expanded in EX to produce shaft work and subsequently electric power by the generator GEN1. The turbine's hot exhaust gases are sent to the HRSG to generate steam at proper temperature and pressure which is then expanded in a series of steam turbines ST that operate at different pressure levels on the principle of the Rankine cycle. A fraction of the steam leaving the turbine can be used as heating utility in the reboiler of the CO_2 capture plant (not shown in Fig. 2) and the remaining fraction is condensed and recycled back to the HRSG.

The configuration of the combined cycle power plants depends on the desired power capacity. Some arrangements include two gas turbines with their own HRSGs providing steam to one steam turbine. Additionally, they can include multiple electric generators. The components of a HRSG can be arranged in different ways depending on the desired application; for instance, for vertical or horizontal flows of hot gases. Additionally, they can operate at multiple pressure levels. Independently of the HRSG configurations, the main advantages of the NGCC power plants over the conventional steam power plants (i.e. boiler and steam turbines) are the flexibility for power production and the relatively inexpensive capital costs.

3. Process modeling

3.1. CO_2 capture plant

3.1.1. Main model assumptions and considerations

– The chemical reaction system consists of reactions (R1)–(R7):

$$2H_2O \leftrightarrow H_3O^+ + OH^- \quad \text{(R1)}$$

$$2H_2O + CO_2 \leftrightarrow H_3O^+ + HCO_3^- \quad \text{(R2)}$$

$$H_2O + HCO_3^- \leftrightarrow H_3O^+ + CO_3^{2-} \quad \text{(R3)}$$

$$H_2O + MEAH^+ \leftrightarrow H_3O^+ + MEA \quad \text{(R4)}$$

$$MEACOO^- + H_2O \leftrightarrow MEA + HCO_3^- \quad \text{(R5)}$$

$$MEA + CO_2 + H_2O \leftrightarrow MEACOO^- + H_3O^+ \quad \text{(R6)}$$

$$CO_2 + OH^- \leftrightarrow HCO_3^- \quad \text{(R7)}$$

Reactions (R1)–(R5) are equilibrium reactions. Reactions (R6) and (R7) are considered as pseudo first order reactions with the aim of considering the effect of the reaction on the mass transfer phenomena through the enhancement factor.

– CO_2 absorption and amine regeneration are performed in packed columns, which are modeled as a cascade of non-equilibrium stages with chemical reactions to compute temperature, flow rate, and composition profiles.
– Mass transfer is described by the two-film resistance theory.
– Reboiler and condenser are considered as equilibrium stages.
– Kent-Eisenberg model is employed to predict the CO_2 solubility in MEA solutions.
– The fugacity coefficients are estimated using the Peng-Robinson EOS for multi-component systems.
– The concept of number of transfer units (NTU)-height of a transfer

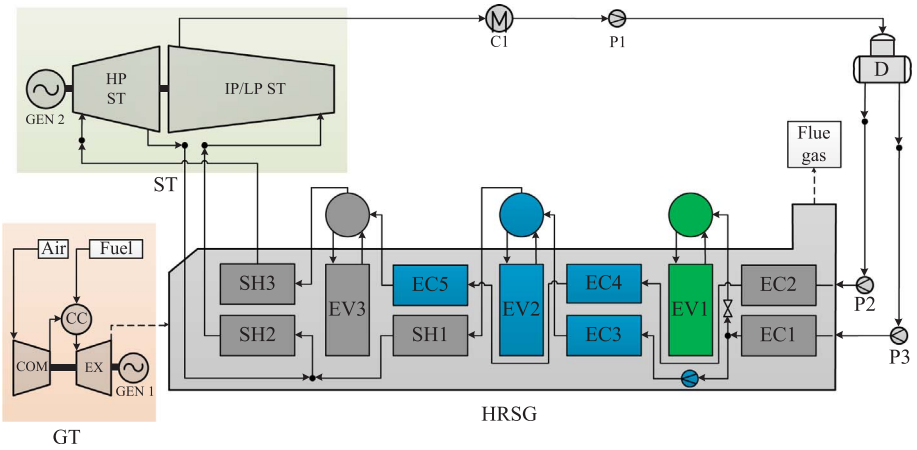

Fig. 2. Schematic of a combined cycle power plant.

unit (HTU) is used to calculate the columns height.
- For a maximum column diameter of 12.8 m, the number of capture trains in parallel to treat the NGCC exhaust combustion gases (which is a model parameter) is assumed to be 6.
- To avoid amine degradation and equipment corrosion, the maximum reboiler temperature is 393 K [113–116].
- Dependence of solubilities, densities, viscosities, diffusivities, fugacity coefficients, and enthalpies with the temperature and composition, estimates of pressure drops along the absorber and regenerator units, and estimates of liquid and mass transfer coefficients are calculated using the state-of-the-art correlations giving by Mores et al. [80,81].
- One intercooled centrifugal compressor with four intercooling stages is involved in the CO_2 compression. The enriched CO_2 stream is compressed from the pressure at the top of the regenerator (which is treated as an optimization variable because it depends on the pressure drop in the regenerator) to 8.6 MPa. Then, the enriched CO_2 stream is pumped up to 14 MPa to allow an efficient transportation.
- Water is removed during the cooling process and is sent back to the CO_2 capture plant to diminish water losses.
- The overall heat transfer coefficients for all heat exchangers are fixed values.

A complete and more detailed description of the model assumptions and considerations for the CO_2 capture plant can be found in previous papers by Mores et al. [78,80,81,83].

3.1.2. Mathematical model

The key equations of the mathematical model are presented in this section. The complete model with the used parameter and constant values are provided as Supplementary data associated with this article.

3.1.2.1. Absorption column. Figs. 3 and 4 show a schematic of the absorption process and a generic absorption stage, respectively. In Fig. 4, for a stage z, the gas stream #41 goes up from stage z − 1 to stage z and the amine solution #44 flows down from stage z + 1 to stage z. The number of stages z is a model parameter but the height of each stage is an optimization variable. The stages z = 1 and z = Z refer to the column bottom and top, respectively. The variables n, T, and P represent the molar flow, temperature, and pressure of each stream; x_i is the molar fraction of component i (MEA, CO_2, H_2O, N_2, and O_2). Based on the made assumptions, the key equations of the rate-based model of the absorption column are:

– Overall mass balance in stage z:

$$n_{41,z-1} + n_{44,z+1} - n_{41,z} - n_{44,z} = 0 \quad (1)$$

– Mass balance for component i in stage z:

$$n_{41,z-1}\cdot x_{41,i,z-1} + n_{44,z+1}\cdot x_{44,i,z+1} - n_{41,z}\cdot x_{41,i,z} - n_{44,z}\cdot x_{44,i,z} = 0\ ,\quad i = \text{MEA},CO_2,H_2O,N_2,O_2 \quad (2)$$

$$\sum_i x_{s,z,i} = 1\ ,\quad i = \text{MEA},CO_2,H_2O,N_2,O_2\ ,\quad s = 41, 44 \quad (3)$$

For stage z = Z:

$$n_{41,z} = n_{42}\ ,\quad z = Z \quad (4)$$

$$x_{41,i,z} = x_{42,i}\ ,\quad z = Z,\quad i = \text{MEA},CO_2,H_2O,N_2,O_2 \quad (5)$$

$$T_{41,z} = T_{42}\ ,\quad z = Z \quad (6)$$

Analogous constraints are properly considered for the stage z < Z.

– Ionic charge relationships in stage z:

$$X_{44,MEAH^+,z} + X_{44,H_3O^+,z} = X_{44,MEACOO^-,z} + X_{44,HCO_3^-,z} + 2\cdot X_{44,CO_3^{2-},z} + X_{44,OH^-,z} \quad (7)$$

$$x_{44,MEA,z} = X_{44,MEAH^+,z} + X_{44,MEACOO^-,z} + X_{44,MEA,z} \quad (8)$$

$$x_{44,CO_2,z} = X_{44,HCO_3^-,z} + X_{44,CO_3^{2-},z} + X_{44,CO_2,z} + X_{44,MEACOO^-,z} \quad (9)$$

X refers to the composition (molar fraction) of each ionic and molecular compound present in the liquid stream.

– Energy balance in stage z:

$$\begin{aligned} &n_{41,z-1}\cdot h_{41,z-1} - n_{41,z}\cdot h_{41,z} \\ &+ n_{44,z+1}\cdot(h_{44,z+1}\cdot x_{44,CO_2,z+1} + \Delta H_{R,44,z+1} + x_{44,H_2O,z+1}\cdot\Delta H_{V,44,H_2O,z+1} + x_{44,MEA,z+1}\cdot\Delta H_{V,44,MEA,z+1}) \\ &- n_{44,z}\cdot(h_{44,z} + x_{44,CO_2,z}\cdot\Delta H_{R,44,z} + x_{44,H_2O,z}\cdot\Delta H_{V,44,H_2O,z} + x_{44,MEA,z}\cdot\Delta H_{V,44,MEA,z}) = 0 \end{aligned} \quad (10)$$

where h is the enthalpy (molar base), and ΔH_R and ΔH_V are the reaction and vaporization heats, respectively. They are calculated using correlations taken from Oyenekan and Rochelle [121] and Hilliard [122], which are included in the Supplementary data associated with this article.

According to the hypothesis of well-mixed condition:

$$T_{44,z} = T_{41,z} \quad (11)$$

– Chemical and phase equilibrium relationships:

Equilibrium constants K_m of reactions (R_1)–(R_5) are calculated by Eqs. (12) and (13), with composition expressed in molar fraction and temperature in Kelvin:

$$K_{m,z} = \prod_j (a_{44,j,z})^{\nu_j} = \prod_j (X_{44,j,z}\cdot\gamma_{44,j,z})^{\nu_j}\ ,\quad m = \text{R1, R2, R3, R4, R5}$$
$$j = \text{MEA},MEAH^+,MEACOO^-,\ CO_2,HCO_3^-,CO_3^{2-},H_3O^+,OH^- \quad (12)$$

$$K_{m,z} = \exp\left(A + \frac{B}{T_{44,z}} + C\cdot\ln(T_{44,z}) + D\cdot T_{44,z} + E\cdot T_{44,z}^2\right),\quad m = \text{R1, R2, R3, R4, R5} \quad (13)$$

where $a_{i,z}$, $\gamma_{i,z}$, and ν_i are the activity, activity coefficient, and stoichiometric coefficient for the component i in the reaction m at the stage z, respectively. As ideal gas behavior is assumed for the liquid phase, the activity coefficients are set to one (Kent-Eisenberg model). The coefficient values used in Eq. (13) are given in Aboudheir et al. [123] and Liu et al. [124].

The equilibrium phase relationships for the reactions (EP1)–(EP3) are estimated by Eqs. (14) and (15):

$$CO_2(g) \leftrightarrow CO_2(aq) \quad (EP1)$$

$$H_2O(g) \leftrightarrow H_2O(l) \quad (EP2)$$

$$MEA(g) \leftrightarrow MEA(aq) \quad (EP3)$$

$$x_{41,i,z}\cdot\varphi_{41,i,z}\cdot P_{41,z} = H_{44,i,z}\cdot\frac{x_{44,i,z}}{\rho_{44,z}}\ ,\quad i = CO_2\ ,\quad m = EP1 \quad (14)$$

$$x_{41,i,z}\cdot\varphi_{41,i,z}\cdot P_{41,z} = p_{44,i,z}\cdot x_{44,i,z}\ ;\quad i = \text{MEA}, H_2O;\quad m = EP2, EP3 \quad (15)$$

where ρ is the molar density (kmol/m^3), P the total pressure (kPa), φ the fugacity coefficient in the gas phase (dimensionless), x the composition of gas and liquid streams (molar fraction), H the Henry's law

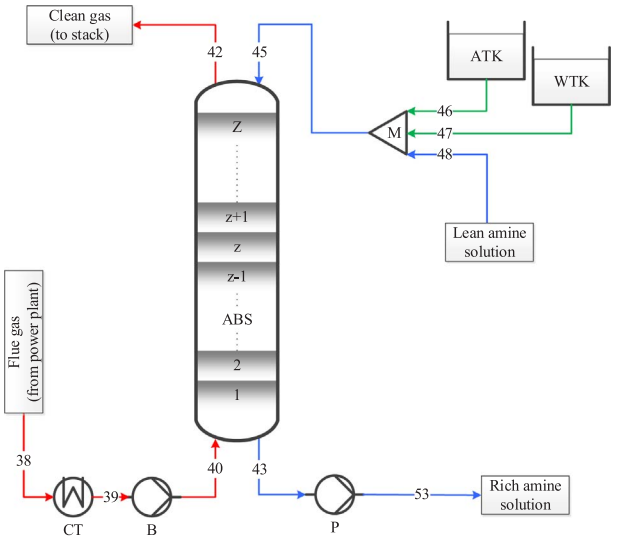

Fig. 3. Schematic of the absorption process.

constant (kPa m^3/kmol), and p the vapor pressure (kPa).

The solubility of CO_2 in MEA solution $H_{44,CO2}$ corrected for the solution ionic strength I is calculated by Eq. (16), which is given in Liu et al. [124] and Greer [125].

$$H_{44,CO_2,z} = 10^{0.152\, I_z}\cdot(x_{44,H_2O,z}\cdot H_{44,CO_2-MEA,z} + x_{44,CO_2,z}\cdot H_{44,CO_2-H_2O,z}) \tag{16}$$

where:

$$H_{44,CO_2-i,z} = \frac{1\times 10^{-3}}{\rho_{44,z}}\exp\left(A + \frac{B}{T_{44,z}} + C\cdot\ln(T_{44,z}) + D\cdot T_{44,z} + E\cdot T_{44,z}^2\right),$$

$$i = MEA, H_2O \tag{17}$$

$$I_z = \frac{1}{2}\frac{\sum_j \psi_j\cdot X_{44,j,z}}{\rho_{44,z}},\quad j = MEAH^+, MEACOO^-, H_3O^+, OH^-, HCO_3^-, CO_3^{-2} \tag{18}$$

where ψ_j is the ion charge.

Vapor pressure (kPa) is calculated by the Antoine expression (Eq. (19)):

$$p_{44,i,z} = \exp\left(A_i + \frac{B_i}{T_{44,z}} + C_i\cdot\ln(T_{44,z}) + D_i\cdot T_{44,z} + E_i\cdot T_{44,z}^2\right),$$

$$i = MEA, H_2O \tag{19}$$

The coefficient values used in Eqs. (13), (17) and (19) are listed in Table A1 in the Supplementary data.

The gas-phase fugacity coefficient φ and the compressibility factor fc of a component k are estimated by Eqs. (20) and (21), respectively, corresponding to the Peng-Robinson EOS for multi-component systems:

$$\ln(\varphi_{k,z}) = \frac{b_{PR,k}}{b_{PR,41,z}}(fc_{41,z}-1) - \ln(fc_{41,z}-B_{PR,41,z}) - \frac{1}{2\cdot\sqrt{2}}\frac{A_{PR,41,z}}{B_{PR,41,z}}\left(\frac{2\cdot\sum_i x_{41,i,z}\cdot a_{PR,i,k,z}}{a_{PR,41,z}} - \frac{b_{PR,k}}{b_{PR,41,z}}\right)\ln\left(\frac{fc_{41,z}-2.414\cdot B_{PR,41,z}}{fc_{41,z}-0.414\cdot B_{PR,41,z}}\right)$$

$$i \neq k,\quad i = MEA, CO_2, H_2O, N_2, O_2 \tag{20}$$

$$fc_{41,z}^3 - (1-B_{PR,41,z})\cdot fc_{41,z}^2 + (A_{PR,41,z} - 3B_{PR,41,z}^2 - 2B_{PR,41,z})\cdot fc_{41,z} - (A_{PR,41,z}\cdot B_{PR,41,z} - B_{PR,41,z}^2 - B_{PR,41,z}^3) = 0 \tag{21}$$

The mixture values A and B are calculated by the mixing rules.

– Design of the absorption column:

The diameter of each stage $D_{ABS,z}$ is calculated by:

$$D_{ABS,z} = \left(\frac{4n_{41,z}}{\pi\cdot f_{ABS,z}\cdot u_{f,ABS,z}\cdot\rho_{41,z}}\right)^{1/2} \tag{22}$$

where u_f is the flooding velocity (m/s) and f is the flooding factor (dimensionless) which ranges from 0.6 to 0.85. The flooding velocity for random packing is calculated according to Leva [126] (Eqs. (23)–(25)).

$$\Upsilon_z = \left(\frac{(u_{f41,z})^2\cdot F_p}{g}\right)\cdot\left(\frac{\rho_{41,z}\cdot MW_{41,z}}{999.53}\right)\cdot f_{2,z}\cdot f_{3,z} \tag{23}$$

$$\Upsilon_z = \exp(-3.7121 - 1.0371\cdot\ln(f_{1,z}) - 0.1501\cdot(\ln(f_{1,z}))^2 - 0.00754\cdot(\ln(f_{1,z}))^3) \tag{24}$$

$$0.01 \leqslant \Upsilon_z \leqslant 10 \tag{25}$$

where MW refers to the molecular weight, μ is the viscosity (Ns/m^2), and F_p (m^2/m^3) is the packing factor (a model parameter).

The design constraint relating the column diameter $D_{ABS,z}$ and the nominal diameter of packing d_p (model parameter) is taken from Seider et al. [127] and Chapel et al. [128]:

$$10\, d_p \leqslant D_{ABS,z} \leqslant 12.8 \tag{26}$$

– Column height:

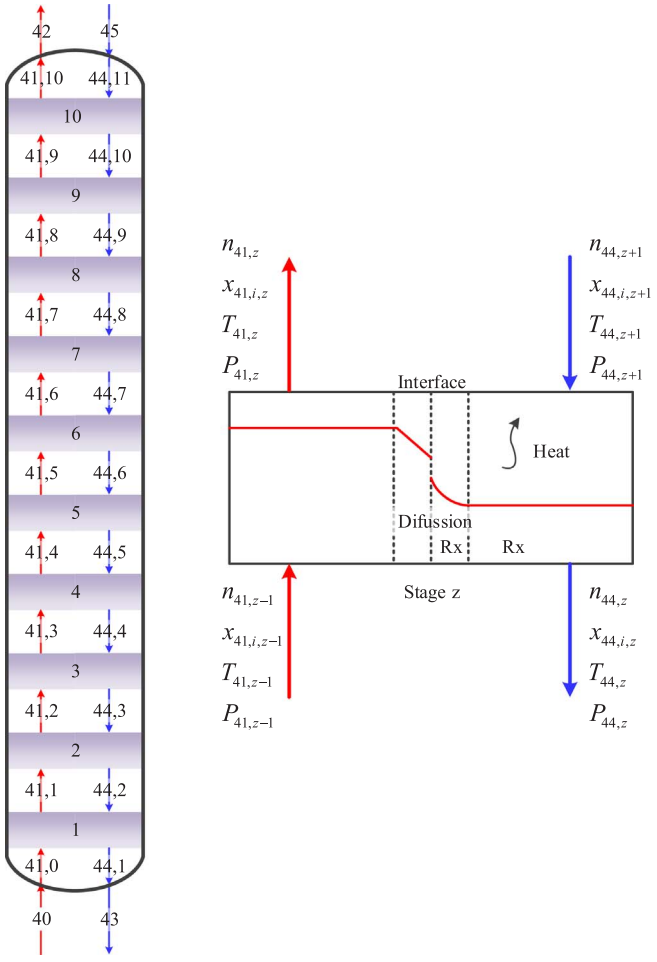

Fig. 4. Schematic of a generic stage z of the absorption column.

The height of the absorption column H_{ABS} depends on the separation requirement $R_{CO2.ABS}$ and the packing efficiency. The NTU-HTU concept is used to calculate the stage height $h_{ABS,z}$:

$$H_{ABS} = \sum_{z=1}^{Z} h_{ABS,z} \tag{27}$$

$$h_{ABS,z} = HTU_z \cdot NTU_z \tag{28}$$

$$HTU_z = \left(\frac{n_{41,z}}{A_{ABS,z} \cdot RT_{41,z} \cdot a_{e,z} \cdot k_{41,z} \cdot \rho_{41,z}}\right) + \Gamma_z \left(\frac{n_{44,z}}{A_{ABS,z} \cdot k_{44,z} a_{e,z} \cdot \rho_{44,z} \cdot E_z}\right) \tag{29}$$

$$NTU_z = -\ln(1-\eta_z) \tag{30}$$

$$\eta_z = \frac{x_{41,CO_2,z} - x_{41,CO_2,z-1}}{x^*_{41,CO_2,z} - x_{41,CO_2,z-1}} \tag{31}$$

The effective interfacial area for mass transfer a_e and the mass transfer coefficients k are calculated by the correlations proposed by Onda et al. [129]. The influence of the reactions (R6) and (R7) on the CO_2 mass transfer is considered by the enhancement factor E:

The corresponding forward constants $k_{r,R6}$ and $k_{r,R7}$ of the parallel and kinetically controlled reactions are taken from Aboudheir et al. [123] and Kucka et al. [130] (Eqs. (33) and (34)):

$$k_{r,R6,z} = 4.495 \times 10^{11} \exp\left(-\frac{44940}{R \cdot T_{44,z}}\right) \tag{33}$$

$$k_{r,R7,z} = \exp\left(31.396 - \frac{6658}{T_{44,z}}\right) \tag{34}$$

– Column pressure drop

The total pressure drop ΔP_{ABS} (kPa) in the absorption column is calculated by Eq. (35):

$$\Delta P_{ABS} = \sum_{z} \Delta P_{ABS,z} \cdot h_{ABS,z} \tag{35}$$

where the pressure drop per unit of packing ΔP_z (kPa/m) is estimated by correlations given by Robbins [131], which consider the pressure drop associated to the dry packing and the liquid presence (Eqs. 3640):

$$\Delta P_{ABS,z} = 0.8160\left(f_{4,z} + 0.4 \cdot f_{4,z}^4 \left(\frac{f_{5,z}}{20000}\right)^{0.1}\right) \tag{36}$$

$$f_{4,z} = 7.4 \times 10^{-8} (10^{2.7 \times 10^{-5} \cdot f_{6,z}^2}) \tag{37}$$

$$f_{5,z} = \left(737.3845 \frac{n_{44,z} \cdot MW_{44,z}}{A_z}\right)\left(\frac{999.53}{\rho_{44,z} \cdot MW_{44,z}}\right)\left(\frac{Fp_d}{64.056}\right)^{0.5}\left(\frac{\mu_{44,z}}{1000}\right)^{0.2} \quad \text{if } Fp_d > 61\ m^2/m^3 \tag{38}$$

$$f_{5,z} = \left(737.3845 \frac{n_{44,z} \cdot MW_{44,z}}{A_z}\right)\left(\frac{999.53}{\rho_{44,z} \cdot MW_{44,z}}\right)\left(\frac{64.056}{Fp_d}\right)^{0.5}\left(\frac{\mu_{44,z}}{1000}\right)^{0.1} \quad \text{if } Fp_d \leqslant 61\ m^2/m^3 \tag{39}$$

$$f_{6,z} = \left(0.8197 \frac{n_{41,z} \cdot MW_{41,z}^{0.5}}{A_z \cdot (\rho_{41,z})^{0.5}}\right)\left(\frac{Fp_d}{64.056}\right)^{0.5} (10^{0.019 \cdot \rho_{41,z} \cdot MW_{41,z}}) \tag{40}$$

Minimum and maximum permissible column pressure drops per unit of packing height are set to ensure a minimum vapor flow rate for avoiding laminar vapor flow and having a well vapor distribution [125,132]:

$$0.08\ kPa/\ m \leqslant \Delta P_{ABS,z} \leqslant 1\ kPa/m \tag{41}$$

– Stream property estimation:

$$h_{41,z} = \sum_i x_{41,i,z} \cdot \int_{298.15}^{T_{41,z}} \left(a_i + b_i \cdot T_{41,z} + c_i \cdot T_{41,z}^2 + d_i \cdot T_{41,z}^3\right) \cdot dT,\ i = MEA, CO_2, H_2O, N_2, O_2 \tag{42}$$

$$h_{44,z} = \sum_i x_{44,i,z} \cdot \int_{298.15}^{T_{44,z}} (a_i + b_i \cdot T_{44,z} + c_i \cdot T_{44,z}^2 + d_i \cdot T_{44,z}^3 + e_i \cdot T_{44,z}^{-2}) \cdot dT, \quad i = MEA, H_2O \tag{43}$$

Enthalpy:

The gas and liquid enthalpies are calculated by Eqs. (42) and (43), respectively, which are taken from Greer [125]:

Viscosity:

The gas and liquid viscosity estimates are based on a logarithmic form of the mixing rule as suggested by Greer [125]. As it is assumed that MEA does not contribute significantly to the overall gas viscosity: $a_{MEA} = b_{MEA} = 0$.

$$\ln(\mu_{41,z}) = \sum_i \ln(x_{41,i,z} \cdot (a_i \cdot T_{41,z} + b_i)),\ i = MEA, CO_2, H_2O, N_2, O_2 \tag{44}$$

Diffusivity:

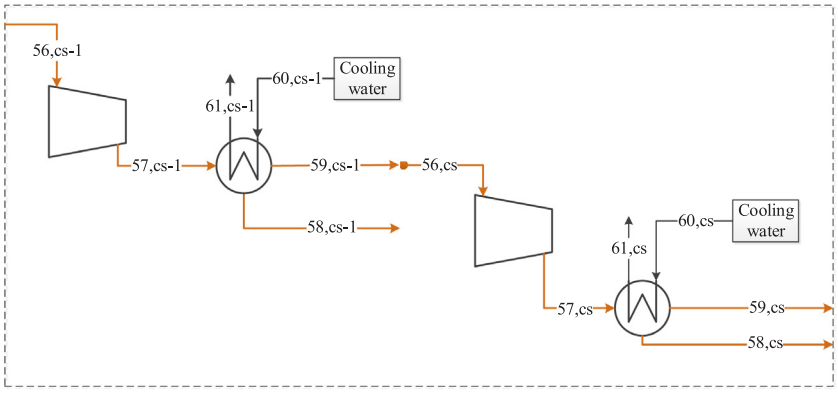

Fig. 5. Schematic of a generic compression stage cs.

Gas diffusivity is calculated by a modified version of the Chapman-Enskog correlation taken from Reid [133]. The estimation of the CO_2 diffusivity in MEA solution is based on the N_2O analogy [134] which corrects the effect of the CO_2-MEA reaction. The expression is given in Versteeg and Van Swaalj [135] and Maceiras et al. [136].

3.1.2.2. Regeneration column. The regeneration column is modeled similarly to the absorption column. The total height of the packing is divided into W stages, in which w = 1 and w = W refer to the column bottom and top, respectively; w = 0 and w = W + 1 refer the reboiler and condenser, respectively, which are modeled as equilibrium stages (i.e. Murphree efficiency is equal to 1). The model involves constraints similar to those used for the absorber, which are included in the Supplementary data.

3.1.2.3. Compressors and blowers. The final compression involves a number of CS intercooled centrifugal compressors (this number is a model parameter). Fig. 5 shows a generic compression stage cs.

The compression power wc (kW) required for a stage cs is estimated by Eq. (45), where γ (=Cp/Cv), fc, and η_{is} are the adiabatic expansion coefficient (model parameter), the gas compressibility factor (estimated using the Peng-Robinson EoS), and the isentropic efficiency of compressor (model parameter), respectively. The exit temperature of the compression stage T_{57} and the total compression power wc_T are calculated by Eqs. (46) and (47), respectively.

$$wc_{cs} = n_{56,cs}\cdot R\cdot T_{56,cs}\cdot fc_{56,cs}\cdot\left(\frac{1}{\eta_{is,cs}}\right)\left(\frac{\gamma_{56,cs}}{\gamma_{56,cs}-1}\right)\left(\left(\frac{P_{57,cs}}{P_{56,cs}}\right)^{1-\frac{1}{\gamma_{56,cs}}}-1\right),$$

$$cs = 1,2...CS \quad (45)$$

$$T_{57,cs}-T_{56,cs} = T_{56,cs}\left(\frac{1}{\eta_{cs}}\right)\left(\left(\frac{P_{57,cs}}{P_{56,cs}}\right)^{1-\frac{1}{\gamma_{56,cs}}}-1\right),$$

$$cs = 1,2...CS \quad (46)$$

$$wc_T = \sum_{cs=1}^{CS} wc_{cs} \quad (47)$$

Connectivity constraints are imposed on molar flows, temperatures, pressures, and compositions (Eqs. (48)–(50)).

$$n_{56,cs} = n_{59,cs-1},\ cs = 2...CS \quad (48)$$

$$P_{56,cs} = P_{59,cs-1},\ cs = 2...CS \quad (49)$$

$$T_{56,cs} = T_{59,cs-1},\ cs = 2...CS \quad (50)$$

The following practical design constraints are considered:

$$T_{57,cs} \leqslant 450.15\ K \quad (51)$$

$$\frac{P_{57,cs}}{P_{56,cs}} = \frac{P_{57,cs-1}}{P_{56,cs-1}} \leqslant 3 \quad (52)$$

3.1.3. CO_2 capture level

The recovery level of the CO_2 captured in the absorber $R_{CO2,ABS}$ (%) and the total recovery level R_{CO2} (%) are calculated by Eqs. (53) and (54), respectively:

$$R_{CO_2,ABS} = 100\cdot\frac{n_{42}\cdot x_{CO_2,42}-n_{40}\cdot x_{CO_2,40}}{n_{40}\cdot x_{CO_2,40}} \quad (53)$$

$$R_{CO_2} = 100\cdot\frac{n_{60}\cdot x_{CO_2,60}}{n_{40}\cdot x_{CO_2,40}} \quad (54)$$

It is important to mention that the mathematical model was verified by comparing the output results with experimental data taken from literature [117,118], with predicted values reported by other authors

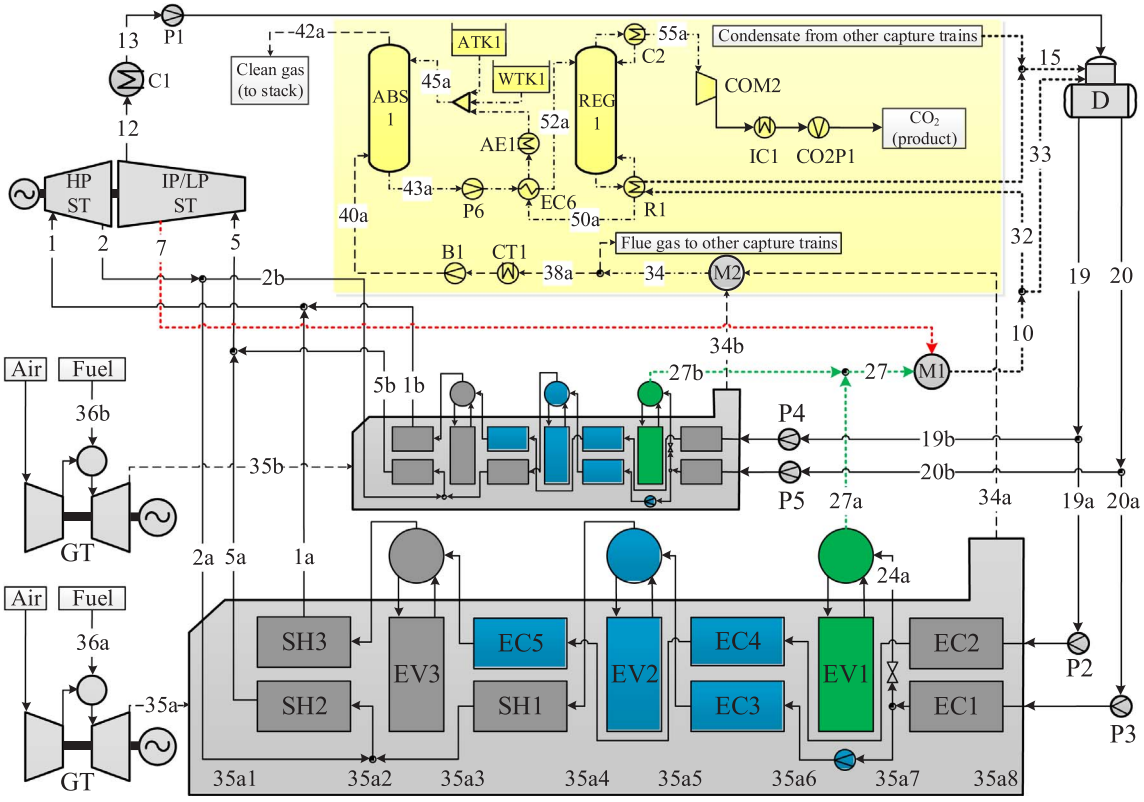

Fig. 6. Schematic indicating the three coupling configurations between NGCC and CO_2 capture plant to be analyzed.

[119,120], and with our simulation studies performed with the process simulator HYSYS. More details on the model verification of the absorption and regeneration columns can be found in Mores et al. [78,80,81].

3.2. Natural gas combined cycle (NGCC) power plant

3.2.1. Main model assumptions and considerations

- The natural gas is assumed to be pure methane [137].
- The pressure ratio in the air compressors and the expander of the gas turbines is fixed.
- The dependence of the ideal gas thermodynamic properties of gaseous streams with temperature and pressure is estimated by correlations taken from Poling et al. [138].
- Complete combustion with excess of air is assumed. CO_2, H_2O, O_2, and N_2 are the components present in the combustion gas stream.
- For the HRSG design: unfired equipment, fixed overall heat transfer coefficients, and neglected pressure drops in the water and steam sides are assumed; geometry and fouling are not considered; heat transfer areas are estimated using the Chen approximation to overcome numerical difficulties arising from the logarithm mean temperature difference (LMTD) computation; steam and water thermodynamic properties are estimated by correlations taken from IAPWS-IF97 [139].
- A single deareator is used, which may be operated by three alternatives: steam (stream #33) and/or hot water (stream #15).

A complete and more detailed description of the model assumptions and considerations for the NGCC power plant can be found in a previous paper by Manassaldi et al. [102].

3.2.2. Mathematical model

In this section, the main equations of the mathematical model are presented. The complete model with the used parameter and constant values are provided as Supplementary data associated with this article.

3.2.2.1. Heat recovery steam generator HRSG. Based on the nomenclature defined in Fig. 6, the energy balance and the heat transfer area for the evaporator EV1 are given by Eqs. (55) and (56), respectively:

$$m_{24a}\cdot(H_{27a}-H_{24a}) = m_{35a}\cdot(H_{35,6,a}-H_{35,7,a}) \tag{55}$$

$$A_{EV1} = \frac{m_{24a}\cdot(H_{27a}-H_{24a})}{U_{EV1}\cdot LMTD_{EV1}} \tag{56}$$

where H, U, and LMTD denote specific enthalpy (kJ/kg), overall heat transfer coefficient (kW/m^2/K), and logarithm mean temperature difference (K), respectively. The latter is calculated as follows:

$$LMTD_{EV1} = \frac{(T_{35,6,a}-T_{27a})-(T_{35,6,a}-T_{24a})}{\ln\left(\frac{T_{35,6,a}-T_{27a}}{T_{35,6,a}-T_{24a}}\right)} \tag{57}$$

A minimum pinch point temperature difference ΔT_{pinch} between the hot and cold streams is imposed by the following constraints:

$$T_{35,7,a}-T_{26a} \geqslant (\Delta T_{pinch})_{EV1} \tag{58}$$

$$T_{35,6,a}-T_{27a} \geqslant (\Delta T_{pinch})_{EV1} \tag{59}$$

Similar constraints are required for the rest of heat exchangers (EC1, EC2, EC3, EV2, EV3, SH1, SH2, and SH3).

3.2.2.2. Steam turbines ST. The high-pressure steam turbine HPST is modeled by Eqs. (60)–(63). The energy balance is given by:

$$m_1\cdot H_1 = m_2\cdot H_2 + W_{HPST} \tag{60}$$

The turbine efficiency η is calculated as follows:

$$\eta_{HPST} = \frac{H_1-H_2}{H_1-H_2^*} \tag{61}$$

by imposing the following constraints:

$$S_1 = S_2^* \tag{62}$$

$$P_1 = P_2^* \tag{63}$$

where S and P denote specific entropy (kJ/kg/K) and pressure (bar), respectively. The asterisk denotes ideal behavior.

Similar constraints are used to model the intermediate and low-pressure steam turbines (IPST and LPST).

3.3. Integration of the CO_2 capture plant with the NGCC power plant

3.3.1. Problem statement

The optimization problem consists of obtaining the best integration arrangement and the optimal operating conditions and process unit sizes that minimize the mitigation cost while satisfying minimum levels of electricity demand (700.0 MW) and CO_2 capture (90%).

3.3.2. Candidate coupling schemes

Fig. 6 illustrates the three candidate coupling configurations to be optimized:

1. A fraction of the steam required in the reboiler R1 of the amine regeneration process of the CO_2 capture plant is provided by the steam turbine IP/LP ST (stream #7 – drawn in red dot line –) and the other fraction by the evaporators of the two HRSGs (streams #27a and #27b which are mixed generating the stream #27 – drawn in green dot line –). This candidate configuration is hereafter referred as C1.
2. All the steam required in the reboiler R1 of the amine regeneration process of the CO_2 capture plant is extracted from the intermediate/low pressure steam turbine IP/LP ST (stream #7). This candidate

Table 1
Optimization variables.

CO_2 capture plant	NGCC power plant
– Pressure, composition, and temperature profiles along the absorber and regenerator units	– Pressure and temperature of fuel, vapor, water, and exhaust gases in the economizer, evaporator, and super-heaters
– Amine and cooling water flow rates	– Vapor, water, and exhaust gases flow rates in the economizer, evaporator, and super-heaters
– Sizes of process units: (1) heat transfer area of condenser, reboiler, MEA cooler, economizer, and inter-stage coolers, (2) packing volume of the absorber and regenerator (both height and diameter)	– Sizes of the HRSGs: heat transfer area of economizers, evaporators, and super-heaters
– Heat loads in the reboiler, condenser, and heat exchangers (amine-amine and amine-cooling water)	– Heat loads in the heat exchangers involved in the HRSGs
– Electric power required by pumps, blowers, and compressors	– Electric power required by compressors and pumps. Electric power produced by the steam turbines
– CO_2 recovery level. A lower bound is imposed to assure a minimum capture target	

Table 2
Capital expenditures (CAPEX) estimation.

Equipment acquisition cost		C_{Inv}
Installation		0.528 C_{Inv}
Instrumentation and control		0.200 C_{Inv}
Piping		0.400 C_{Inv}
Electrical		0.110 C_{Inv}
Building and services		0.100 C_{Inv}
Yard improvements		0.100 C_{Inv}
Services facilities		0.200 C_{Inv}
Land		0.050 C_{Inv}
Total direct manufacturing cost	DMC	2.688 C_{Inv}
Engineering		0.100 DMC
Construction expenses		0.100 DMC
Contractor's fee		0.005 DMC
Contingencies		0.170 DMC
Total indirect manufacturing cost	IMC	0.375 DMC
Investment on fix capital	IFC	DMC + IMC
Working investment		0.250 IFC
Start-up cost + initial MEA cost		0.100 IFC
Capital expenditures	CAPEX	1.350 IFC = 5 C_{Inv}

configuration is hereafter referred as C2.

3. All the steam required in the reboiler R1 of the amine regeneration process of the CO_2 capture process is provided by the evaporators of the two HRSGs (streams #27a and #27b which are mixed generating the stream #27). This candidate configuration is hereafter referred as C3.

3.3.3. Mathematical optimization model

Formally, the optimization problem to be solved for each candidate coupling scheme can be mathematically expressed as follows:

$$\begin{aligned} &\text{Minimize MC} \\ &\text{s.t. :} \\ &\mathbf{h}_s(\mathbf{x}) = \mathbf{0},\ \forall s \\ &\mathbf{g}_t(\mathbf{x}) \leqslant \mathbf{0}\ ,\ \ \forall\ t \\ &W_{net} \geqslant 700\ \text{MW} \\ &R_{CO_2} \geqslant 90\% \end{aligned} \tag{P1}$$

where MC is the mitigation cost or the CO_2 avoided cost (objective function to be minimized); $\mathbf{x}$ is the optimization variable vector (Table 1); $\mathbf{h}_s(\mathbf{x})$ refers to equality constraints (mass, energy, and momentum balances; correlations to estimate physico-chemical properties; and expressions for process unit design); and $\mathbf{g}_t(\mathbf{x})$ refers to inequality constraints, which are used, for instance, to avoid temperature cross situations, and to impose lower and upper bounds on some critical operating variables. W_{net} and R_{CO2} are the required total net electric power generation and CO_2 recovery, respectively.

As a result, the proposed optimization problem provides:

- Minimal mitigation cost (MC).
- Optimal temperature, pressure, composition, and flow rate of all process streams.
- Optimal heat transfer area (HTA) of all process units.
- Optimal electric power generated by each steam turbine.
- Optimal contribution of the cost items to the capital expenditures (CAPEX), operating expenditures (OPEX), and total annual cost (TAC).

The mitigation cost represents a normalized measure of the electric power generation cost with respect to the amount of captured CO_2 [140–142], which is calculated as follows:

$$MC = \frac{COE_{PP+CP} - COE_{SAPP}}{E_{SAPP} - E_{PP+CP}} \tag{64}$$

where COE refers to the cost of electric power generation – expressed in \$/(MWh) – and E is the amount of CO_2 emitted per unit of total net electric power generated – expressed in t_{CO2}/(MWh) –, evaluated for two different scenarios: (i) the NGCC power plant coupled to the CO_2 capture plant – denoted by the subscript PP + CP –, and (ii) the NGCC power plant operating in a standalone mode i.e. without CO_2 capture – denoted by the subscript SAPP – which is the reference plant configuration. In the published papers, a same reference plant configuration is used independently from the configuration of the power plant that is being studied, i.e. the same reference values of COE_{SAPP} and E_{SAPP} are used for evaluating the mitigation cost of different power plant configurations. Unlike the published papers, it is here proposed that the reference values used in Eq. (64) change accordingly with the integration configuration (NGCC and CO_2 power plant) that is being considered, or, in other words, that the (four) values of COE_{PP+CP}, COE_{SAPP}, E_{PP+CP} and E_{SAPP} correspond to the same configuration of the NGCC plant.

The amount of CO_2 emitted per unit of generated energy E – expressed in t_{CO2}/(MWh) – is calculated using Eq. (65):

$$E = \frac{3.6}{W_{net}}\left(1 - \frac{R_{CO_2}}{100}\right)\cdot x_{CO_2}^{34}\left(\frac{MW_{CO_2}}{MW^{34}}\right)\cdot m^{34} \tag{65}$$

where R_{CO2} is the CO_2 capture level; $x_{CO2}{}^{34}$ and m^{34} refer to the CO_2 molar fraction (mol/mol) and mass flow rate (kg/s), respectively, of the stream #34 with the exhaust gases leaving the power plant and entering the capture plant. MW_{CO2} and MW^{34} refer to the molecular weight of CO_2 and gaseous mixture in the stream #34, respectively. W_{net} is the generated total net electric power (MW), which is calculated using Eq. (66):

$$\begin{aligned} W_{net} = &\sum_{i=1}^{N_{GT}} (W_{GT} - W_C^{PP})_i + \sum_{l=1}^{N_{ST}} W_{ST} - \sum_{j=1}^{N_P^{PP}} (W_P^{PP})_j \\ &- \sum_{k=1}^{N_{CT}} (W_P^{CP} + W_C^{CP} + W_B^{CP})_k \end{aligned} \tag{66}$$

where the first and second summations refer to the net electric power generated by the gas turbines GT and the steam turbines ST, respectively; the third summation accounts the total electric power consumed by pumps P in the NGCC power plant PP; and the last term accounts for the total electric power required by pumps P, blowers B, and compressors C in the CO_2 capture plant CP. N_{GT}, N_{ST}, N_P, and N_{CT} refer to the number of gas turbines (2), steam turbines (1), pumps which depends on the configuration, and CO_2 capture trains (6), respectively.

The cost for the generated electric power (COE) is calculated using Eq. (67), where TAC is the total annual cost (\$/yr.):

$$COE = \frac{TAC}{W_{net}\,\tau} \tag{67}$$

where τ is the working hours per year (8000 h/yr.).

The total annual cost is calculated using Eq. (68), which includes the capital expenditures (CAPEX) annualized by a capital recovery factor (CRF) and the annual operating expenditures (OPEX):

$$TAC = \frac{CAPEX}{CRF} + OPEX \tag{68}$$

The CAPEX includes the costs of the process units and the costs associated to the design and construction of the necessary facilities and auxiliary services. The last cost items are calculated in terms of the total investment cost (C_{inv}) through an economic index f_1 (=5), as expressed by Eq. (69). The specific cost values used to determine the economic index f_1 involved in Eq. (69) are listed in detail in Table 2, which are assumed according to the guidelines given by Abu-Zahra et al. [140] and Rao and Rubin [142].

$$CAPEX = f_1 \cdot C_{INV} \tag{69}$$

The capital recovery factor (CRF) is calculated using Eq. (70) assuming an interest rate (i) of 8% and a project lifespan (n) of 25 years [83,143]:

Table 3
Reference costs (C_0^k) used to compute the cost items.

Equipment	Unit	Cost	Characteristics
Gas turbines	M$/kW	0.00026	SGT5-4000F
Steam turbine	M$/kW	0.00026	3 pressure levels
Steam generators (HRSG)	M$/kW	0.01115	Horizontal, unfired
CO_2 pump	M$/kW	0.90960	Centrifugal, CS
Vessel of absorber/ regenerator	M$/m^2	0.06781	Vertical vessel, SS
Compressor	M$/kW	0.04200	Centrifugal, SS
Reboiler	M$/m^2	0.01476	Kettle, SS-SS
Blower	M$/kW	0.01338	Centrifugal (turbo), CS
Economizer	M$/m^2	0.01026	Floating head, SS-SS
Packing column	M$/m^3	0.01047	Intalox Saddles, ceramic
Condenser, cooler, intercoolers	M$/m^2	0.00708	Floating head, CS-SS
MEA pump	M$/kW	0.00574	Centrifugal, SS
Tank	M$/m^3	0.00447	Floating roof, CS
Raw materials and utilities	Unit	Cost	
Cooling water	$/t	0.0509	
MEA make-up	$/t	1858	
Fuel	$/GW	3.318	

$$CRF = \frac{i(1+i)^n}{(1+i)^n - 1} \quad (70)$$

The total investment cost (C_{inv}) is calculated by Eq. (71) as the sum of the individual acquisition cost (C_{inv}^k) of the pieces of equipment (k) of the power plant and the capture system, which depends on their sizes (X^k) and constructive characteristics, as expressed by Eq. (72):

$$C_{inv} = \sum_k C_{inv}^k \quad (71)$$

$$C_{inv}^k = C_0^k (X^k)^a \quad (72)$$

where the exponent a is assumed equal to 1.0 for turbines and 0.6 for the capture plant equipment and HRSGs. The reference costs (C_0^k) are calculated using correlations reported in the literature [144–148]. Table 3 lists all the pieces of equipment considered to calculate the total capital investment including the numerical values of the reference costs which were updated considering the 2014 CEPCI indexes [149].

The operating expenditures (OPEX), which are calculated using Eq. (73), include the cost of raw materials and utilities (C_{rm}), maintenance (C_{mant}), manpower (C_{mp}), and other costs related to the total investment cost (C_{inv}). In Eq. (73), the specific cost values used to determine the economic indexes f_2 (=2.2) and f_3 (=0.33) are listed in Table 4, which are assumed according to the guidelines given by Abu-Zahra et al. [140] and Rao and Rubin [141].

$$OPEX = C_{rm} + C_{mant} + f_2 \cdot C_{mp} + f_3 \cdot C_{inv} \quad (73)$$

The costs of raw materials and utilities (C_{rm}) are calculated using Eq. (74) as a function of their annual consumption (m^u), specific cost (C_{rm}^u) and the working hours per year (τ); specifically, the consumptions of fuel, cooling water, and MEA are considered in Eq. (74). A nominal loss of 1.5 kg of MEA per tonne of CO_2 is assumed [141,150]. In addition, an extra 20% of the cost of the nominal loss of MEA is considered for the corrosion inhibitor cost [141]. The specific costs of the cooling water, MEA, and fuel are also listed in Table 3, which were taken from Rao and Rubin [141], U.S. Department of Energy [151], and Ulrich and Vasudevan [152], respectively.

$$C_{rm} = \tau \cdot \sum_u C_{rm}^u m^u \quad (74)$$

The resulting NLP model was implemented in GAMS (General Algebraic Modeling System) and solved using the CONOPT 3 [153], which is based on a generalized reduced gradient method. It is highly nonlinear and non-convex with a great number of variables and constraints (3444 variables and 3582 equality and inequality constraints), which can lead to convergence problems or convergence to local optima. Hence, an efficient procedure for initialization of variables is required to solve the optimization model. To this end, variable and equation are scaled and a systematic procedure consisting of a pre-processing phase for variable initialization followed by an optimization phase is applied, which succeeded to converge the optimization model of the NGCC plant [47,102] and the CO_2 capture plant [78] individually.

The pre-processing phase consists in solving a sequence of submodels which increase in complexity and number of constraints and variables, in which the solution obtained by a submodel provides initial values for variables to solve the following submodel. The pre-processing phase begins by solving the mass and energy balances of the entire process using initial guess values for temperature, pressure, composition, and flow rate of the main process streams assigned by the user externally. It is desired to reduce, as much as possible, the number of initial guess values to be assigned externally. This is done, for instance, by initializing enthalpy and entropy of the superheated steam in terms of the corresponding initial guess values for temperature and pressure using the same model correlations; then, these initial values for enthalpies are used to initialize the electric power generated in the steam turbines. The application of this procedure to the rest of the variables allows to obtain a feasible solution in a few iterations and to facilitate the convergence of this (first) submodel to an optimal solution. The objective function is the maximization of the total net power generation, requiring the generation of at least 700 MW (design specification given through a lower bound value). The pre-processing phase continues by adding the design constraints of the NGCC and CO_2 capture plants; the resulting (second) submodel is solved without any external

Table 4
Operating expenditures (OPEX) estimation.

Raw material and utility	C_{rm}	
Operative manpower	C_{mp}	
Maintenance	C_{mant}	
Local taxes		0.02 IFC
Insurance		0.01 IFC
Supervision and support labor	C_S	0.30 C_{mp}
Laboratory charges		0.10 C_{mp}
Operative supplies		0.01617 IFC
Plant overhead		0.45 (C_{mp} + C_S) + 0.04851 IFC
Total production cost	PC	C_{rm} + C_{mant} + 1.985C_{mp} + 0.0947 IFC
Administrative		0.13 C_{mp}
Distribution and marketing		0.00397 C_{mp}
Research and development		0.0397 C_{mp}
Total additional cost	AC	0.217 C_{mp}
Operative expenditures	OPEX	PC + AC = C_{rm} + C_{mant} + 2.2 C_{mp} + 0.33 C_{inv}

Table 5
Parameter values assumed for the CO_2 capture plant.

Parameter	Units	Value
Number of capture trains		6
Minimum CO_2 capture target	%	90
Fresh amine composition	% w/w	30
Fresh amine temperature	K	298.15
Reboiler pressure	kPa	200
Compression pressure	MPa	8.6
CO_2 pumping pressure	MPa	14
Minimum cold flue gas temperature	K	313.15
Packing properties		
Type		Intalox saddles
Specific area	m^2/m^3	118
Nominal packing size	M	0.05
Critical surface tension	N/m	0.061
Void fraction	%	79
Dry packing factor	m^2/m^3	121.4
Overall heat transfer coefficients		
Economizer	$W/m^2/K$	760.8
Condenser	$W/m^2/K$	320.2
Reboiler	$W/m^2/K$	1360.3
MEA cooler	$W/m^2/K$	1005
Inter-stage coolers	$W/m^2/K$	277.7

Table 6
Parameter values assumed for the NGCC power plant.

Parameter	Units	Value
Net electricity production (minimum)	MW	700
Number of gas turbines/HRSGs	–	2/2
Gas Turbine		
Fuel LHV	kJ/kmol	802518
Fuel composition (CH_4)	%	100
Fuel temperature	K	298.15
Maximum fuel pressure	kPa	1215.9
Pressure ratio	–	18.2
Isentropic efficiency of compressors	–	0.95
Isentropic efficiency of turbines	–	0.863
Maximum inlet temperature in GT	K	1500
Minimum air excess (mole basis)	%	220
Air inlet (ISO condition)	kPa/K	101.3/288.15
Steam Cycle		
Isentropic efficiency of steam turbines	–	0.9
Minimum pinch point	K	15
Approach point	K	5
Minimum heat transfer temp. difference	K	15
Minimum feed water temp. at HRSG	K	333.15
Overall heat transfer coefficient		
Economizer	$W/m^2/K$	42.6
Evaporator	$W/m^2/K$	43.7
Superheater	$W/m^2/K$	50

Table 7
Reference values corresponding to the stand-alone power plant (SAPP) configurations required in Eq. (64) to compute the MC for the coupled (PP + CP) configurations.

Parameter	Units	SAPP configurations		
		C1	C2	C3
CO_2 emissions per unit of generated energy (E) [a]	kg/MWh	328.1561	333.1158	331.4891
Cost of electricity (COE) [b]	$/MWh	56.54	56.66	56.38
Net power output (W_{net}) [a]	MW	875.62	862.59	866.82
Thermal efficiency [a]	%	60.15	59.25	59.54
Total annual cost (TAC) [b]	M$/yr.	396.06	391.01	390.95
Operating expenditures (OPEX) [b]	M$/yr.	273.66	271.02	270.88
Capital expenditures (CAPEX) [b]	M$	1306.59	1280.93	1281.72

[a] Numerical values taken from Manassaldi et al. [102].
[b] Values calculated from Manassaldi et al. [102].

initial guess value since the new variables in the design constraints depend only on the variables of the previous submodel, and consequently, they are initialized using the values obtained previously. These previous values are also used to set tight lower and upper bounds by reducing and increasing them in a given percentage, respectively. Like the previous submodel, the objective function is the maximization of the net electric power generation. The pre-processing phase finishes by adding the cost constraints; the resulting (third) submodel is solved without any external initial guess value, obtaining the solution corresponding to the complete model (NGCC + CO_2 capture plant); similarly, the net electric power generation is minimized.

In the optimization phase, the complete model is solved using the last values as initial values but considering the minimization of the mitigation cost as the objective function, thus obtaining the desired optimal solution for the entire process.

It is worth mentioning that all optimization problems were solved at a low computational cost when the described initialization strategy (pre-processing phase) was applied; convergence problems were found when the complete model was solved using a “random” or non-systematic initialization. The obtaining of global optimal solutions cannot be guaranteed due to the non-convex nature of the formulated problem and that a local search optimization algorithm was employed, as mentioned in Section 3.3.3.

4. Discussion of results

The model parameter values for the CO_2 capture plant and the NGCC power plant used in the optimizations are listed in Tables 5 and 6, respectively. Table 7 lists the reference values corresponding to the stand-alone power plant (SAPP) configurations – C1, C2 y C3 described in Section 3.3.2 – to compute the mitigation cost (Eq. (64)) that results from the optimization of the three coupled (PP + CP) configurations. These reference values were taken from Manassaldi et al. [102] by maximizing the overall efficiency and calculating the corresponding cost items.

4.1. Optimization results

4.1.1. Optimal integration configuration

The optimization problem P1 stated in Section 3.3.3 was solved for each coupling scheme C1, C2, and C3. A minimum mitigation cost value of 90.88 $/t CO_2 was computed, and corresponds to the coupling scheme C1, which is represented in Fig. 7 with the optimal values of the flow rate, pressure, and temperature of each stream, as well as the heat transfer area in each economizer, evaporator, and superheater, and the electric power produced in the gas and steam turbines. This optimal solution is referred as OS. The second column in Table 8 also indicates the corresponding optimal values of TAC, OPEX, CAPEX, and COE for OS. The second column in Table 9 indicates the contribution of each process unit to CAPEX and each operating parameter to OPEX, ordered by the decreasing degree of relevance.

As it can be observed in Table 8 for OS, the contributions of the TAC and COE are 493.44 M$/yr. and 82.84 $/MWh, respectively, implying increases of 24.58% and 46.51%, respectively, with respect to the reference NGCC power plant (Table 7) (from 396.06 to 493.44 M$/yr., and from 56.54 to 82.84 $/MWh, respectively). The contributions of CAPEX and OPEX to TAC are 1870.84 M$ and 318.18 M$/yr., respectively, implying an increase in 43.18% and 16.26% with respect to the reference values (from 1306.59 to 1870.84 M$ and from 273.66 to 318.18 M$/yr., respectively).

Regarding the OPEX distribution, Table 9 indicates that the cost associated with fuel consumption is the largest contributor with 87.55% (139.56 M$/yr.), followed by the cooling water with 8.02% (12.79 M $/yr.), and MEA make-up and inhibitor with 4.37% (6.963 M$/yr.).

In Table 9, it can also be seen that around 70% of CAPEX corresponds to the investments required by the gas turbines ($\approx$ 40%) and by

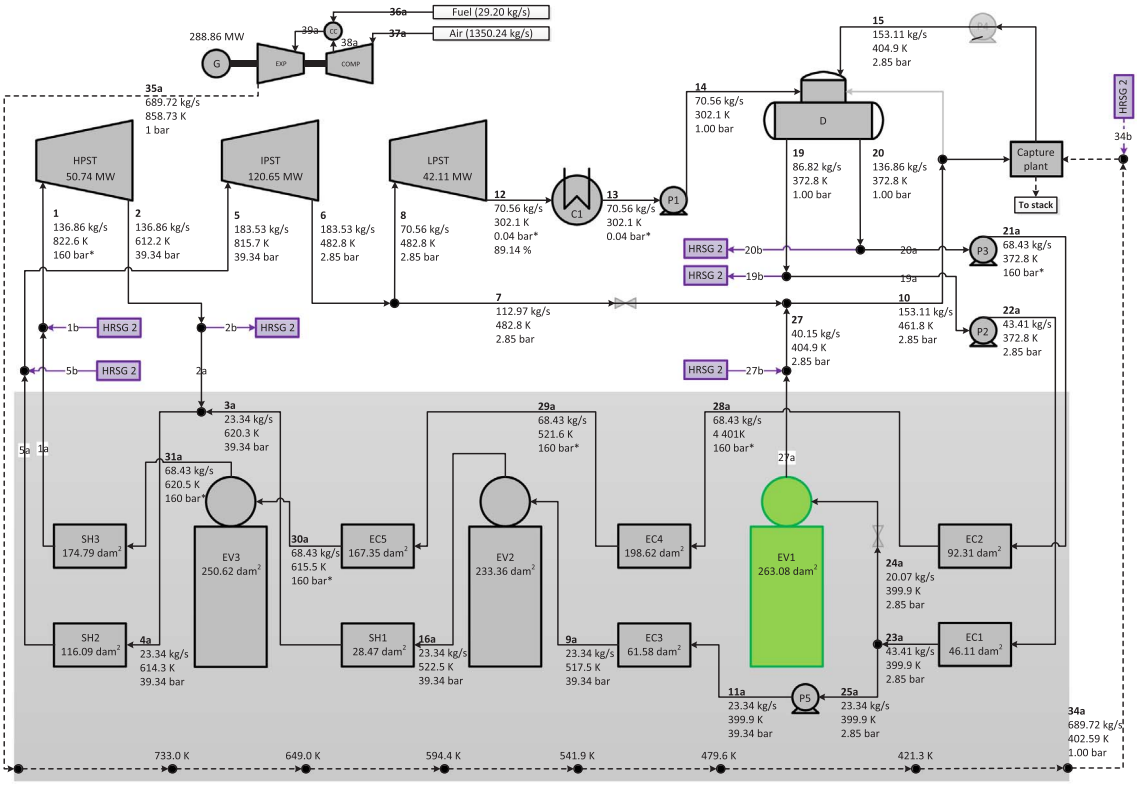

* Optimal variable values that reached their lower/upper bounds.

Fig. 7. Results corresponding to the optimal integration configuration OS (C1).

Table 8
Optimal values of MC, TAC, OPEX, CAPEX, and COE.

	OS	SOS1	SOS2
Mitigation cost (MC), $/t CO_2	90.88	91.02	102.34
Total annual cost (TAC), M$/yr.	493.44	491.58	484.24
Operating expenditures (OPEX), M$/yr.	318.18	317.60	316.47
Capital expenditures (CAPEX), M$	1870.84	1857.30	1790.95
Cost of electricity (COE), $/MWh	82.84	83.42	86.10

Table 9
Contributions of the cost items to the total raw material and utility cost and total equipment acquisition cost.

	OS	SOS1	SOS2
Raw material and utility cost, M$/yr.			
Total	159.40	159.81	163.63
Fuel	139.56 (87.55%)	139.56 (87.33%)	139.56 (85.29%)
Cooling water	12.79 (8.02%)	13.20 (8.26%)	17.02 (10.40%)
MEA make up and inhibitor, $/yr.	6.963 (4.37%)	6.961 (4.36%)	6.959 (4.25%)
H_2O make-up, $/yr.	0.0913 (0.06%)	0.0924 (0.06%)	0.0948 (0.06%)
Equipment acquisition cost, M$			
Total	374.16	371.45	358.23
Gas turbines	149.22 (39.88%)	149.22 (40.17%)	149.22 (41.65%)
Absorption columns	55.84 (14.92%)	56.21 (15.13%)	56.56 (15.79%)
Steam turbines	55.15 (14.74%)	53.29 (14.35%)	44.62 (12.46%)
Compressors	37.65 (10.06%)	37.64 (10.13%)	37.63 (10.50%)
Heat recovery steam generators	29.93 (8.00%)	28.74 (7.74%)	23.78 (6.64%)
Regeneration columns	12.03 (3.22%)	12.12 (3.26%)	12.30 (3.43%)
Blowers	9.79 (2.62%)	10.06 (2.71%)	10.29 (2.87%)
Economizer	6.80 (1.82%)	6.63 (1.78%)	6.48 (1.81%)
Condensers	5.48 (1.46%)	5.42 (1.46%)	5.39 (1.50%)
Reboilers	5.26 (1.41%)	5.18 (1.39%)	5.10 (1.42%)
Amine-water exchangers	1.98 (0.53%)	1.93 (0.52%)	1.82 (0.51%)
CO_2 pumps	1.66 (0.44%)	1.66 (0.45%)	1.66 (0.46%)
MEA tanks	1.51 (0.40%)	1.51 (0.41%)	1.51 (0.42%)
Intercoolers	1.38 (0.37%)	1.37 (0.37%)	1.37 (0.38%)
H_2O tanks	0.24 (0.06%)	0.24 (0.06%)	0.24 (0.07%)
MEA pumps	0.24 (0.06%)	0.23 (0.06%)	0.23 (0.06%)

the absorber columns and steam turbines which contribute almost equally to CAPEX with around 15% each. The contribution of compressors is greater than the HRSGs (10.06 and 8.00%, respectively), which is in turn greater than the contribution of the amine regeneration columns (3.22%). The blowers and economizers are the seventh and eighth largest contributors to CAPEX (2.62 and 1.82%, respectively), followed by the condensers and reboilers which contribute with around 1.40% each.

As shown in Fig. 7, the optimal solution indicates that the (total) steam mass flow rate required by the CO_2 capture process is 153.11 kg/s at 2.856 bar, of which 112.97 kg/s is provided by IP-LP ST and 40.15 kg/s by EV1. The total electric power generated by the two gas turbines is 577.71 MW (288.86 MW each) and by the steam turbines is 213.50 MW with the optimal distribution among HPST, IPST, and LPST shown in Figs. 7 and 8b. The electric power required by pumps and blowers in the NGCC power plant and CO_2 capture plant is 2.48 and 44.21 MW, respectively.

Regarding the optimal distribution of the total heat transfer area among the heat exchangers, Fig. 8a shows that around 60% of the total area (1632.40 dam^2) is distributed among the three evaporators (EV1, EV2, and EV3) and the economizer EC4. The evaporator EV1, which produces a fraction of the steam required by the CO_2 capture plant, is the process unit that demands the largest heat transfer area (16.11%), followed by EV3 (15.35%), EV2 (14.29%), and EC4 (12.16%). Around

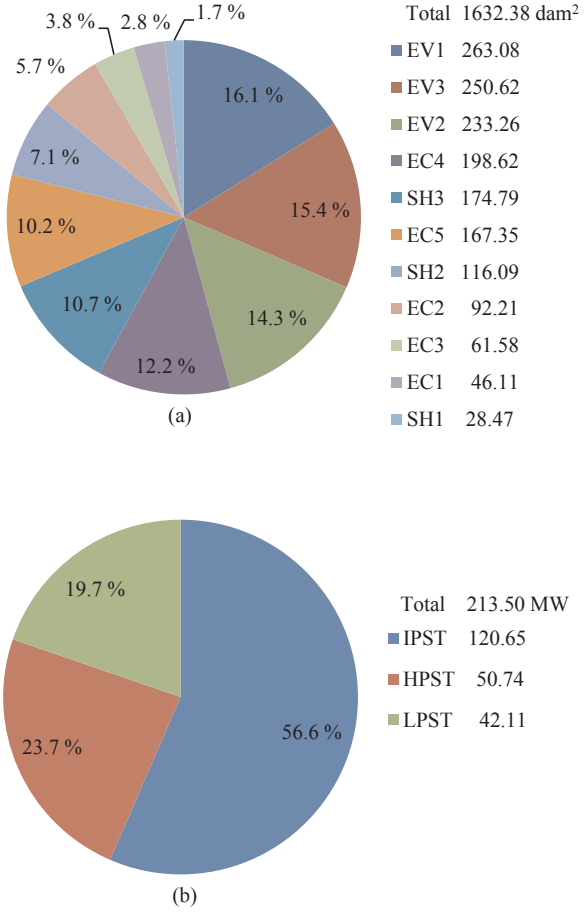

Fig. 8. Optimal distribution obtained for OS: (a) heat transfer area, (b) electric power generated in the steam turbines.

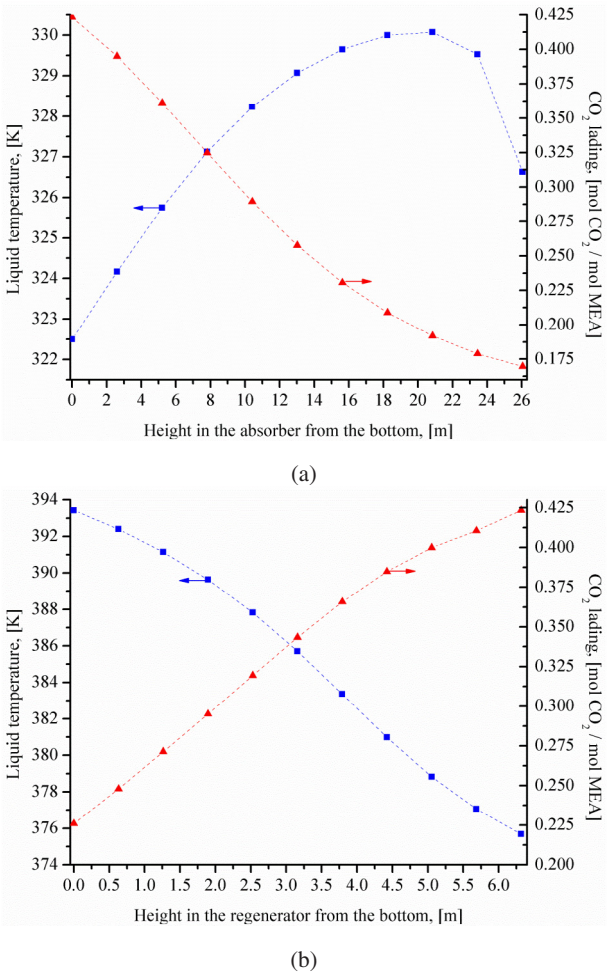

Fig. 9. Optimal profiles of the liquid temperature and CO_2 loading: (a) absorber, (b) regenerator.

20% of the total heat transfer area is almost equally distributed between the superheater SH3 and the economizer EC5. The remaining 20% is distributed among the rest of the superheaters (SH2: 7.11% and SH1: 1.74%) and economizers (EC2: 5.65%, EC3: 3.77%, and EC1: 2.82%).

Finally, Fig. 9 depicts the liquid temperature and the CO_2 loading profiles in both the absorption column and the amine regeneration column. The reaction heat and the evaporation heat are the main parameters that affect the temperature of the liquid and gas phases. Fig. 9a shows that the temperature of the liquid phase increases from 326.4 K (at the column entrance) to a maximum value of 330 K at 18.23 m because of the heat released by the exothermic reaction between CO_2 and MEA. Thus, in this section of the absorber, the liquid phase – where the chemical reactions take place – increases the temperature as the solvent reacts with CO_2 as a consequence of the combined effect of the exothermic reaction and the water vaporization. The temperature remains substantially uniform in the column section comprised between 18.23 and 23.4 m, and then starts to decrease because of the energy transfer from the liquid phase to the gas phase flowing in counter-current. At 26.05 m the temperature reaches 326.6 K.

With regard to the amine regeneration column, Fig. 9b clearly shows, as expected, that the temperature of the liquid phase monotonously decreases from the column bottom, where the temperature is at a maximum and corresponds to the boiling point temperature. Regarding the CO_2 loading in the liquid phase (α_{CO2}) in the absorber, Fig. 9a shows how it increases from the top column section (26.05 m) to the bottom (0 m). Indeed, as the flue gas reacts with MEA, the CO_2 concentration in the liquid phase increases and the MEA concentration decreases, leading to an increase in α_{CO2} from the column top to the bottom. Contrarily, in the amine regeneration process, α_{CO2} decreases from the top of the regenerator (6.23 m) obtaining the lean-amine solution at the bottom of the regeneration column (Fig. 9b).

4.1.2. *Suboptimal integration configurations*

The objective of this section is to analyze and compare the variations of the mitigation cost, the operating conditions, and the process unit sizes of the other (suboptimal) coupling configurations described in Section 3.3.2 with respect to the optimal configuration SO. The first examined suboptimal solution – which is referred as SOS1 – corresponds to the configuration C2, where the total steam required by the reboiler of the CO_2 capture process is only supplied by the steam turbine IP/LP ST. The second suboptimal configuration examined corresponds to the case in which the total steam required by the reboiler of the CO_2 capture process is only taken from the evaporator EV1 (coupling scheme C3); this solution is referred as SOS2.

Figs. 10 and 12 show the optimal values of the flow rate, pressure, and temperature of each stream, as well as the heat transfer area in each economizer, evaporator, and superheater, and the electric power generated in the gas and steam turbines for solutions SOS1 and SOS2, respectively. Figs. 11a and 13a illustrate the optimal distribution of the total heat transfer area among the heat exchangers for SOS1 and SOS2, respectively; while Figs. 11b and 13b show the electric power generated by the steam turbines and its optimal distribution among HPST, IPST, and LPST, for SOS1 and SOS2, respectively.

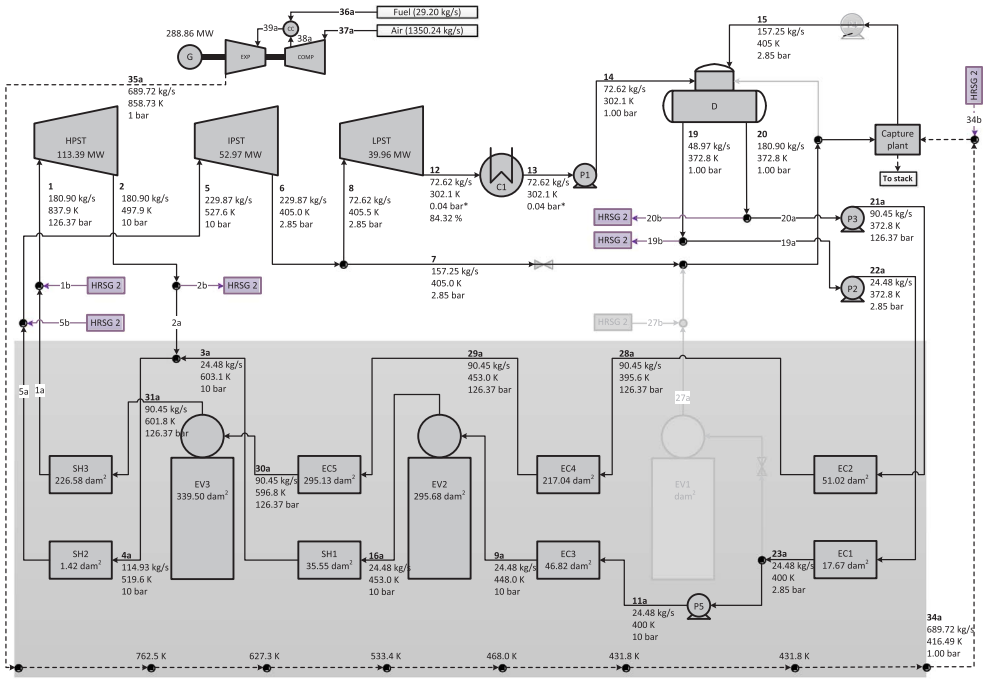

Fig. 10. Results corresponding to the suboptimal integration configuration SOS1 (C2).

* Optimal variable values that reached their lower/upper bounds.

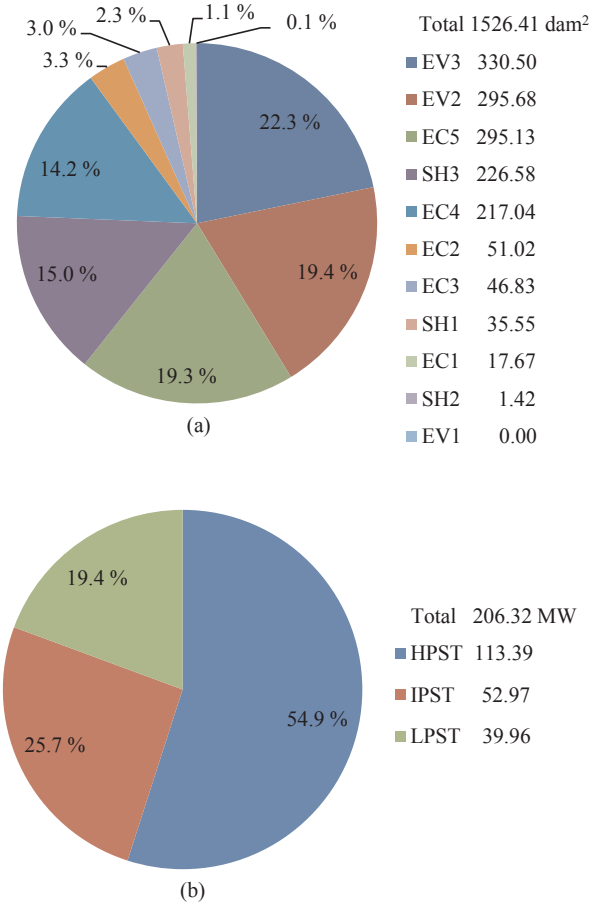

Fig. 11. Optimal distribution obtained for SOS1: (a) heat transfer area, (b) electric power generated in the steam turbines.

4.1.3. Comparison between the optimal and suboptimal solutions

Tables 10 and 11 summarize the main optimization results obtained for the NGCC and CO_2 capture plants, respectively, for the three coupling configurations. Next, the suboptimal solutions SOS1 and SOS2 are compared with the optimal solution OS.

4.1.3.1. Optimal OS vs. suboptimal solution SOS1. Table 8 shows that the mitigation cost obtained by SOS1 is only 0.15% higher than OS (91.02 vs. 90.88 \$/t CO_2). This is because the TAC for SO is only 0.38% higher than SOS1 (493.44 vs. 491.58 M\$/yr.) and the COE_{PP+CP} for SOS1 is 0.70% higher than OS (83.42 vs. 82.84 \$/MWh). In addition, the total net electric power generated by SOS1 is only 1.4% lower than OS. The amount of emitted CO_2 is the same in both cases since the flue gas comes from the same gas turbine type (full load) and the CO_2 capture level is fixed at 90%. Even though the relationships among the computed values result in practically similar mitigation costs for both OS and SOS1, significant differences can be observed between them, not only on the operating conditions (flow rates, pressures, temperatures) but also in the sizes of the heat exchangers in the HRSG and steam turbines. Thus, the result comparison indicates that it is possible the existence of two different integrated process configurations – with different requirements of total heat transfer area and different levels of electric power generation by the steam turbines – with almost equal mitigation cost. Indeed, the solution SOS1 (configuration C2) which does not include the EV1 in the HRSG – unlike the solution OS (configuration C1) – determines a reduction in the total heat transfer area with respect to OS of around 106 dam^2 (from 1632.40 to 1526.41 dam^2) resulting in the generation of 7.92 MW of electric power less than OS (736.61 vs. 744.53 MW) but leading to almost equal mitigation cost.

Fig. 14 compares the T–Q diagrams corresponding to the solution OS (Fig. 14a) and SOS1 (Fig. 14b). The graphical comparison clearly shows that the inclusion of the evaporator EV1 in OS increases the degrees of freedom of the optimization problem allowing to distribute the heat loads, driving forces (temperatures of the working fluid and gas), and heat transfer areas along the HRSG more conveniently, so as to achieve a greater net power generation. The gas temperature at the exit of the HRSG computed for OS is around 14 K lower than SOS1 (402.6 K in Fig. 14a vs. 416.5 K in Fig. 14b) and, since the gas flow rate is the same in both cases, the total heat transferred in the HRSG obtained for OS is 8 MW greater than SOS1.

The results reported in Table 12 indicate that EC5 is the heat

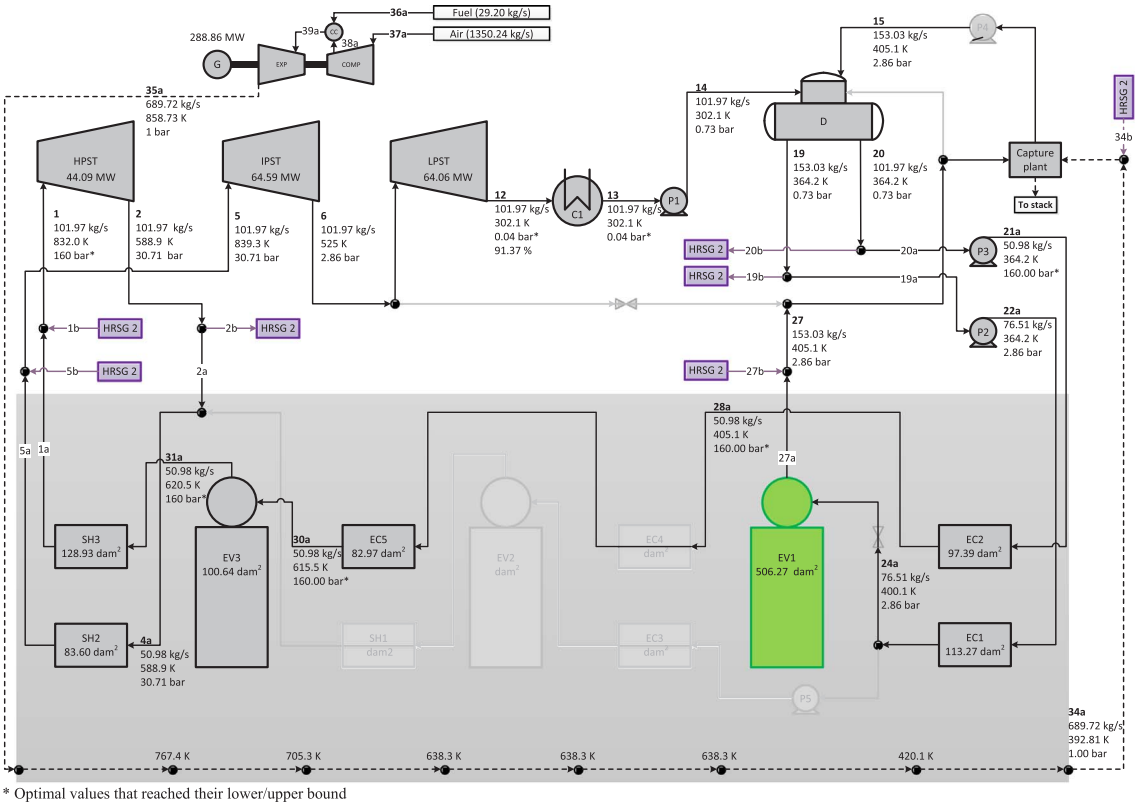

* Optimal values that reached their lower/upper bound

Fig. 12. Results corresponding to the suboptimal integration configuration SOS2 (C3).

exchanger of the HRSG with the largest percentage increase in the heat transfer area (76.35%, from 167.35 dam^2 for SO to 295.13 dam^2 for SOS1), followed by EV3 which increases its size by 35.0% (from 250.62 to 339.50 dam^2). The area increase in EC5 is mainly due to the increased heat load (36.08 vs. 64.57 MW) since the driving force in both cases is practically the same (51 K) although the temperature values of each stream are different. More precisely, the heat load in EC5 increases from 36.08 to 64.57 MW because the flow rate of the working fluid increases from 68.43 to 90.45 kg/s and the difference of temperatures increases from ≈94 K (615.5 K–521.6 K) to ≈144 K (596.8 K–453 K) while the difference of temperatures of the gas stream increases from ≈54 K (649.0 K–594.4 K) to ≈94 K (627.3 K–533.4 K). Similarly to EC5, the area increase in EV3 is due to the heat load in it, but the effect in EV3 is greater than in EC5 since the driving force in EV3 computed by SOS1 is greater than OS (72.5 vs. 60.9 K) – the driving force in EC5 is practically the same for OS and SOS1 (51 K).

The process units SH3, EV2, and SH1 also increase their heat transfer areas by 29.62, 26.70, and 24.86%, respectively. Similarly to EC5, the LMTD in these process units remain virtually constant; therefore, the area increases are due to the increases of the heat loads. Finally, EC4 is the process unit that increases less its heat transfer area (9.27%). The LMTD and the heat load in it behave conversely to the rest of the process units; its area increases from 19.86 to 21.20 dam^2 because the LMTD and the heat load decrease from 35.41 to 22.25 K and from 41.8 to 24.06 MW, respectively.

The heat transfer areas of SH2, EC1, EC2, and EC3 computed by SOS1 are significantly reduced compared to OS. The variations of the LMTD values and the heat loads contribute positively to decrease the area of SH2, EC1, and EC2; while in EC3 the decrease of the heat load is more important than the increase in the LMTD. In this sense, SH2 is the heat exchanger that shows the greatest percentage reduction of the heat transfer area, which is by around 98% (116.09 vs. 1.42 dam^2), followed by EC1, EC2, and EC2 with 61.67, 44.73, and 23.96% reduction, respectively.

Regarding the steam turbines, the mass flow rate and the temperature of the working fluid at the entrance of the high-pressure steam turbine (HPST) computed by SOS1 increase 32.18% (from 136.86 to 180.90 kg/s) and 1.86% (from 822.6 to 837.9 K) with respect to OS, respectively, while the pressure decreases by around 21% (from 160 to 126.37 bar). These variations determine an increase in the generated electric power of 62.66 MW (from 50.74 to 113.39 MW), which represents a 123.47% increase. However, although the flow rate of the circulating fluid increases from 185.53 to 229.87 kg/s in the intermediate-pressure steam turbine (IPST), the inlet temperature and pressure decrease from 815.7 to 527.6 K, and from 39.34 to 10.0 bar, respectively, resulting in a decrease of the generated electric power of 67.68 MW (from 120.65 to 52.97 MW), which represents a 56.1% reduction. On the other hand, at the entrance of the low-pressure steam turbine (LPST), the mass flow rate of the working fluid computed by SOS1 increases from 70.56 to 72.62 kg/s and the temperature decreases from 482.8 to 405.5 K with respect to OS. The pressures at the entrance and outlet of LPST are the same in both cases (2.85 and 0.04 bar, respectively). These operating conditions in LPST determine a slightly decrease of the generated electric power in SOS1 of 2.15 MW (from 42.11 to 39.96 MW). The difference of the generated electric power obtained by OS and SOS1 in each steam turbine can be observed by comparing Figs. 7 and 10 or Figs. 8a and 11b.

Regarding the CO_2 capture plant, Table 11 lists the optimal values of the main variables that result from each integration configuration. Despite the listed variables are model optimization variables, it can be observed that only a few of them vary. Among the operating variables, the values of the lean solvent flow rate and rich solvent CO_2 loading vary more than the lean and rich solvent temperatures and the lean solvent CO_2 loading. Table 11 shows that the values obtained in SOS1 are lower than OS, except for the rich solvent CO_2 loading. The variable showing the greatest percentage variation is the lean solvent flow rate (4.7%), followed by the rich solvent CO_2 loading (2.7%). Among the design variables, the regenerator height is the variable with the greatest

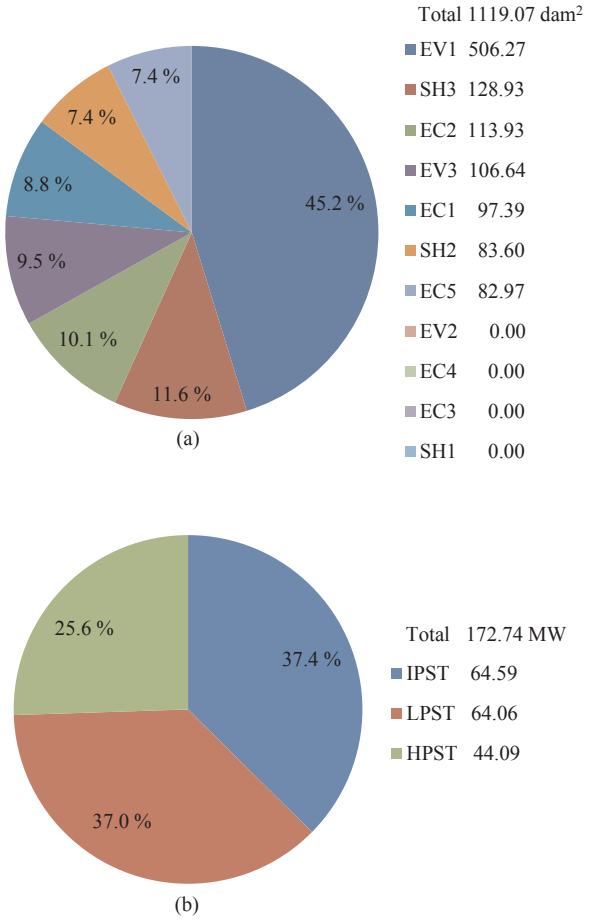

Fig. 13. Optimal distribution obtained for SOS2: (a) heat transfer area, (b) electric power generated in the steam turbines.

percentage variation (12.81%) which increases from 6.32 to 7.12 m, followed by the absorber height (4.45%) which increases from 26.05 to 27.22 m. The MEA cooler, economizer, reboiler, and condenser also decrease their heat transfer areas by around 4.31, 4.20, 2.66, and 1.76%, respectively.

The pressure drop values in the absorption and regeneration columns increase from 11.12 to 11.72 kPa, and from 2.29 to 2.60 kPa, respectively, as a result of the variation of the column height and flow rate, and transport properties of the streams.

Finally, the comparison of the temperature profiles in the absorption column depicted in Fig. 15a allows to see that the maximum temperature for SOS1 is 1–2 K lower than OS, and that it is predicted for OS at 21.7 m from the bottom.

4.1.3.2. Optimal solution OS vs. suboptimal solution SOS2. In contrast to the result comparison between OS and SOS1, the mitigation cost for the suboptimal solution SOS2 is 12.61% higher than OS (102.34 vs. 90.88 \$/t CO_2). Compared to OS, Tables 8 and 10 indicate that the COE_{PP+CP} value is increased by 3.93% (86.10 vs. 82.84 \$/MWh) while the TAC value, the net electric power generated, and the thermal efficiency decrease by 1.86% (484.24 vs. 493.44 M\$/yr.), 5.51% (703.00 vs. 744.53 MW), and 5.57% (48.13 vs. 50.97%), respectively. Compared to SOS1, the COE_{PP+CP} value increases by 3.21% (86.10 vs. 83.42 \$/MWh) while the TAC value, the net electric power generated, and the thermal efficiency decrease by 1.49% (484.24 vs. 491.58 M\$/yr.), 4.48% (703.00 vs. 736.61 MW), and 4.56% (48.13 vs. 50.43%), respectively.

It is interesting to observe in Table 8 that, despite the TAC obtained for C1 is higher than the obtained for C2 and C3, the corresponding MC for C1 is lower than C2 and C3. This is explained by the fact that the W_{net} in C1 increases more rapidly than the TAC, thus resulting in a lower value of the cost of electricity COE_{PP+CP} according to Eq. (67): 82.84 vs. 83.42 and 86.10 \$/MWh. On the other hand, the amount of CO_2 emitted per unit of generated energy E_{PP+CP} in C1 is lower than C2 and C3: 38.72 vs. 39.14 and 41.01 kg/MWh, respectively. Then, as in Eq. (64) (COE_{PP+CP} – COE_{SAPP}) decreases more rapidly than the corresponding decrease of (E_{SAPP}- E_{PP+CP}), the resulting MC for C1 is lower than for C2 and C3.

Table 9 shows that the total equipment acquisition cost computed

Table 11
Comparison of the main optimization variables of the CO_2 capture plant.

	Units	OS (conf. C1)	SOS1 (conf. C2)	SOS2 (conf. C3)
Operating variables				
Lean solvent flow rate	mol/s	9987.94	9583.2	9158.9
Lean solvent temperature	K	326.63	326.54	326.43
CO_2 loading (lean solvent)	–	0.1789	0.1771	0.1742
Rich solvent temperature	K	378.05	377.32	376.42
CO_2 loading (rich solvent)	–	0.423	0.4322	0.4417
Design variables				
Reboiler duty	MW	58.43	56.83	55.30
Electric power	MW	7.37	7.50	7.62
Condenser area	m^2	3294.30	3236.22	3200.85
Inter-stage coolers area	m^2	329.55	328.13	326.16
MEA cooler area	m^2	602.90	576.87	522.47
Economizer area	m^2	2546.76	2437.78	2347.52
Reboiler area	m^2	904.79	880.73	858.34
Absorber height	m	26.05	27.21	28.52
Absorber diameter	m	11.00	10.95	10.88
Absorber pressure drop	kPa	11.12	11.72	12.37
Regenerator height	m	6.32	7.12	8.08
Regenerator diameter	m	3.37	3.31	3.26
Regenerator pressure drop	kPa	2.29	2.60	2.95

Table 10
Comparison of the main optimization variables of the NGCC power plant.

	Units	OS (conf. C1)	SOS1 (conf. C2)	SOS2 (conf. C3)
Total electric power produced in GT	MW	577.71	577.71	577.71
Total electric power produced in ST	MW	213.50	206.33	172.74
Electric power required in NGCC	MW	2.48	2.42	1.72
Electric power required in capture plant	MW	44.21	45.01	45.73
Net power output	MW	744.53	736.61	703.00
Thermal efficiency	%	50.97	50.43	48.13
Total heat transfer area in each HRSG	dam^2	1632.38	1526.41	1113.07
Total heat duty in each HRSG	MW	357.64	347.25	364.93
Steam used in capture plant	kg/s	153.11	157.25	153.03
CO_2 emissions per unit of generated energy	kg/MWh	38.72	39.14	41.01

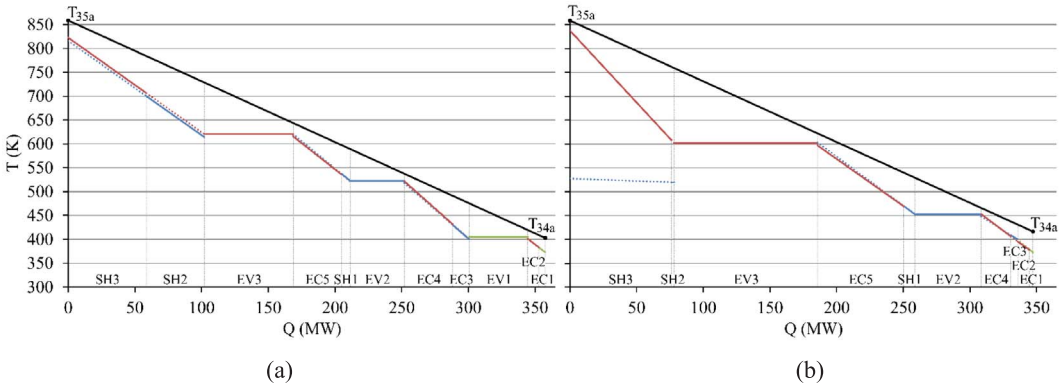

Fig. 14. T–Q diagrams corresponding to (a) solution OS (conf. C1) and (b) solution SOS1 (conf. C2).

Table 12
Optimal values of HTA for OS, SOS1, and SOS2 with the percentage variation with respect to OS.

Unit	OS	SOS1		SOS2	
	HTA (dam^2)	HTA (dam^2)	Variation (%)	HTA (dam^2)	Variation (%)
EV1	263.08	0	–	506.27	92.43↑
EC5	167.35	295.13	76.35↑	82.97	50.42↓
EV3	250.62	339.50	35.00↑	106.64	57.45↓
SH3	174.79	226.58	29.62↑	128.93	26.23↓
EV2	233.36	295.68	26.70↑	0	0
SH1	28.47	35.55	24.86↑	0	0
EC4	198.62	217.04	9.27↑	0	0
SH2	116.09	1.42	98.80↓	83.60	27.98↓
EC1	46.11	17.67	61.67↓	97.39	111.21↑
EC2	92.31	51.02	44.73↓	113.27	22.70 ↑
EC3	61.58	46.82	23.96↓	0	0
Total	1632.64	1526.41	6.51↓	1119.07	31.46↓

for SOS2 decreases 4.25% with respect to OS (from 374.16 to 358.23 M$) as a result of a reduction of the investment cost of most process units, except for the absorber and blowers, which slightly increase their investment cost with respect to OS (from 55.84 to 56.56 M$, and from 9.79 to 10.29 M$, respectively). It can also be noted that the order of relevance of the contribution of each piece of equipment to CAPEX for SOS2 remains unchanged with respect to OS and SOS1.

Compared to OS, OPEX computed for SOS2 decreases from 318.18 to 316.47 M$/yr. since the decrease of the electricity cost in the NGCC power plant is more significant than the increase in the costs associated with the cooling water and H_2O make-up (Table 9). The comparison of the results presented in Table 10 allows to see that the total heat transfer area of the HRSG computed for SOS2 is 519.33 dam^2 smaller than OS (1113.07 vs. 1632.40 dam^2), in spite of the HRSG heat duty in SOS2 is slightly higher than OS (around 7.3 MW) because the temperature of the gas stream leaving the HRSG is 10 K lower (392.81 vs. 402.6 K) – as a given mass flow rate is assumed according to the specification for the considered SGT5-4000F taken from catalogue. In SOS2, the deletion of EV2, and consequently of SH1, EC3, and EC4, implies only one pressure level for electric power generation using the same vapor flow rate in all steam turbines (101.97 kg/s; Fig. 12) unlike OS where 136.86 kg/s is used in HPST, 183.53 kg/s in IPST, and 70.56 kg/s in LPST (Fig. 7). The fact of using only one evaporator (EV3) for electric power generation implies that 45.8% of the total energy available in the HRSG is used to generate the steam required for amine regeneration in the CO_2 capture plant (167.5 of 365.1 MW), compared to the 12.3% required in OS (43.9 of 357.31 MW), while 197.6 MW is used for electric power generation compared to 313.41 MW used in OS, resulting in a lower electric power generation. The values of electric power generated by HPST, IPST, and LPST in SOS2 (Fig. 12) are 44.09, 64.59, and 64.06 MW, respectively, which are more evenly distributed

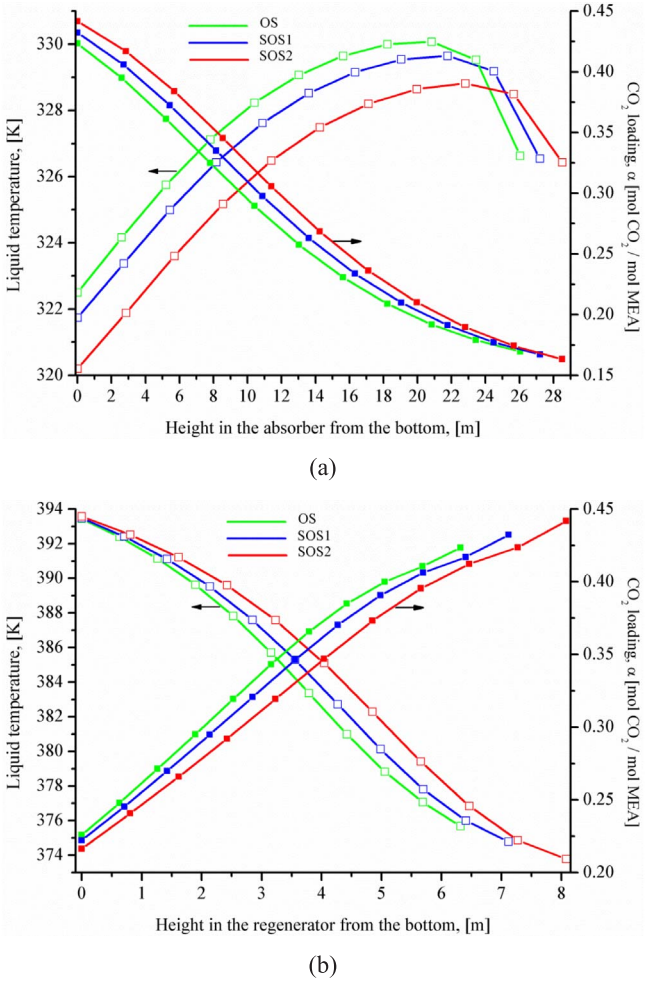

Fig. 15. Liquid temperature and CO_2 loading profiles: (a) absorber, (b) amine regenerator.

than in OS (Fig. 7), where 50.74, 120.65, and 42.11 MW of electric power are generated by HPST, IPST, and LPST, respectively.

Fig. 16 compares the T–Q diagrams for the solutions OS and SOS2. It clearly shows that the energy available in the gas stream is more conveniently transferred to the HRSG when EV2, and consequently SH1, EC3, and EC4 are included into the integrated process configuration i.e. for OS solution (config. C1, Fig.16a). In other words, for the employed cost model (functionalities and unitary cost values) and considered optimization criterion (minimization of the mitigation cost), although the TAC value for OS is higher than SOS2 due to an increase in the total

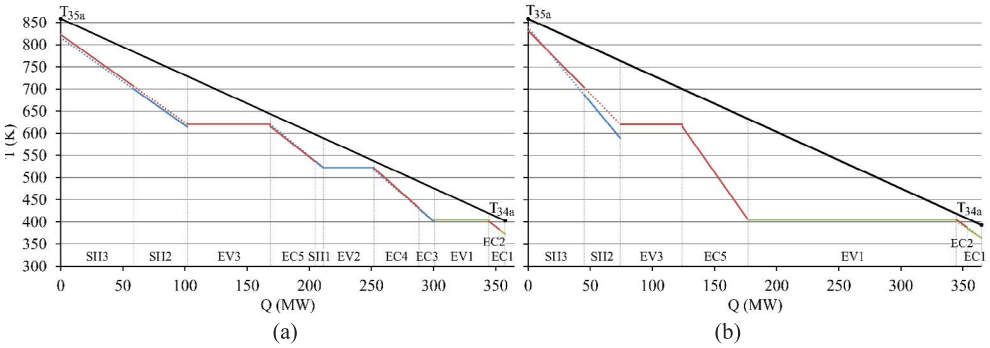

Fig. 16. T–Q diagrams corresponding to (a) solution OS (conf. C1) and (b) solution SOS2 (conf. C3).

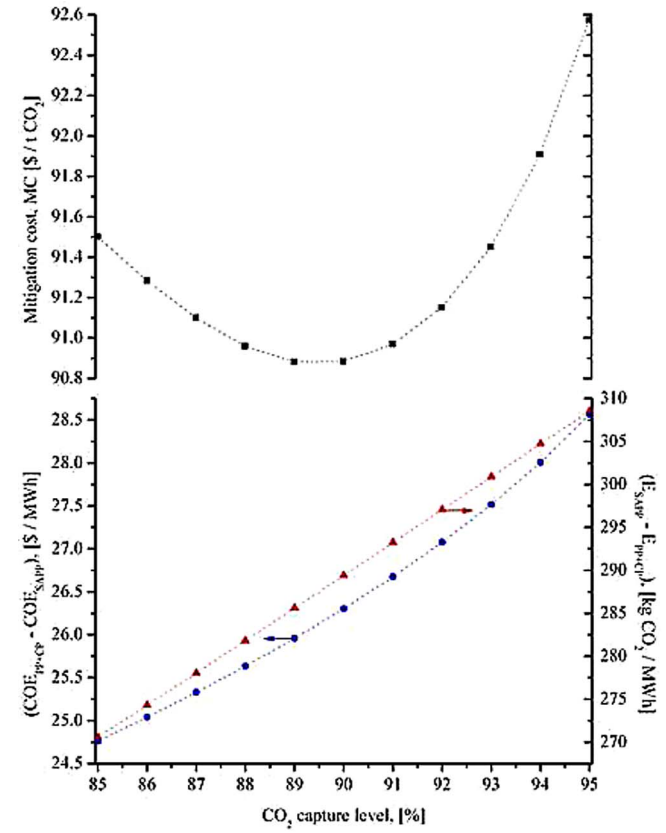

Fig. 17. Influence of the CO_2 capture level on the mitigation cost and total net electric power output for the optimal configuration C1.

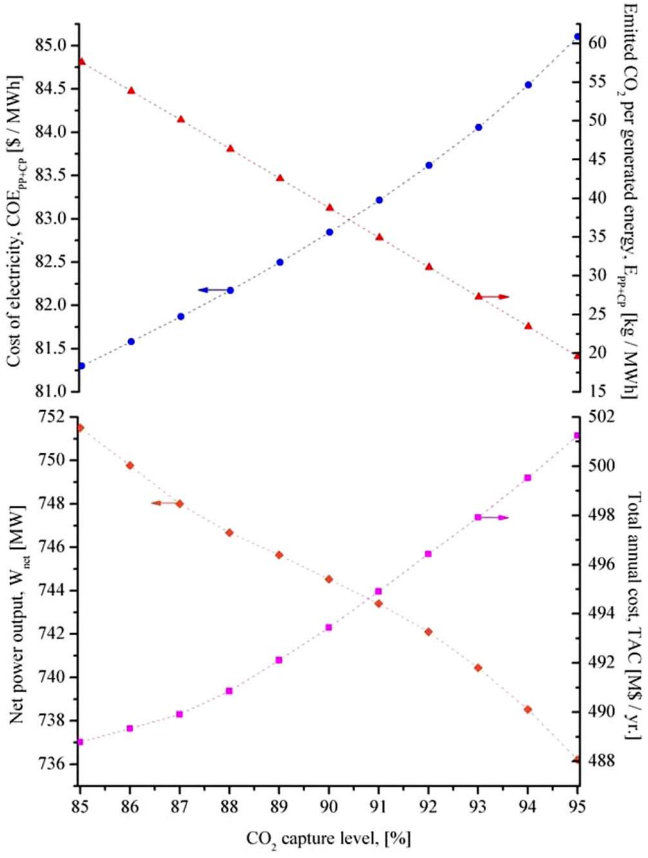

Fig. 18. Influence of the CO_2 capture level on the cost of electricity COE and the amount of CO_2 emitted per unit of generated energy E for the optimal configuration C1.

heat transfer area (i.e. a higher CAPEX), the total net electric power generated in OS is sufficiently higher than SOS2 to determine a lower COE_{PP+CP} value, and thus a lower mitigation cost value.

Regarding the HRSG design, it is worth noting the opposite tendencies that follow the percentage variation of the heat transfer area of each exchanger in SOS1 and SOS2 with respect to OS (Table 12). According to the obtained values, it can be observed that, if the heat transfer area of a process unit in SOS2 increases with respect to OS, then it decreases in SOS1, and vice versa.

Finally, the optimization models were also solved for interest rates of 12, 13, 14, and 15%, and amortization periods of 10, 15, and 20 years, which are more appropriate than 8% and 25 years, respectively, for a private investor in the utility space. For the all considered pairs of values, the same optimal coupling scheme i.e. configuration C1 was obtained and a similar comparative trend between the optimal solutions for the three configurations was observed when the mitigation cost is minimized.

4.1.4. *Influence of the CO_2 capture level on the mitigation cost and process integration configuration*

The developed NLP models were also solved to study the variation of the mitigation cost and to find the optimal configuration when the CO_2 capture level is parametrically varied from 85 to 95%. As a result from the process configuration point of view, the same optimal process integration configuration – i.e. C1 – was obtained for all the examined CO_2 capture levels.

The results are illustrated in Figs. 17 and 18 in terms of the difference of the cost of electricity (COE_{PP+CP} – COE_{SAPP}), the difference of the amount of CO_2 emitted per unit of generated energy (E_{SAPP} – E_{PP+CP}), the total annual cost (TAC), and the net power output (W_{net}), which are the most influential variables on the mitigation cost (MC).

Depending on the trade-offs among these variables, it may be possible to obtain a W_{net} higher than 700 MW (minimal target design specification) if this is beneficial to minimize the MC (Eq. (64)). Indeed, this is what happens in the optimal configuration C1, as shown in

Fig. 18.

It can also be observed in Fig. 18 that the W_{net} decreases when the CO_2 capture level increases. This is as a consequence of the fact that more steam is conveyed from the NGCC to the amine regeneration – because of the higher CO_2 recovery levels – thus resulting in a decrease of the W_{net}. On the other hand, the TAC increases when the CO_2 capture level increases because of the increase in the size of the capture plant (Fig. 18). Thus, both the decrease of W_{net} and the increase in the TAC lead to an increase in the cost of electricity (COE_{PP+CP}), as shown in Fig. 18. In addition, with increased capture levels, the amount of CO_2 emitted decreases more rapidly than the W_{net} resulting in a decrease of E_{PP+CP} (Fig. 18). These variations lead to increasing both (COE_{PP+CP} – COE_{SAPP}) and (E_{SAPP} – E_{PP+CP}) with increased values in the CO_2 capture level but with different functionalities: linear for (E_{SAPP} – E_{PP+CP}) and nonlinear for (COE_{PP+CP} – COE_{SAPP}). The difference (COE_{PP+CP} – COE_{SAPP}) increases more rapidly than the difference (E_{SAPP} – E_{PP+CP}) as shown in Fig. 17, leading to a minimal MC value of 90.88 \$/t CO_2 at a CO_2 capture level of 89%. At the minimum, the computed W_{net}, COE_{PP+CP}, and E_{PP+CP} values are 745.64 MW, 82.49 \$/MWh, and 51.04 t CO_2/MWh, respectively (Fig. 18). At the minimum, the computed W_{net}, COE_{PP+CP}, and E_{PP+CP} values are 745.64 MW, 82.49 \$/MWh, and 51.04 t CO_2/MWh, respectively.

5. Conclusions

This paper addressed the optimization of integrated natural gas combined cycle and CO_2 capture plants using mathematical programming and rigorous optimization approaches. The aim was to determine the optimal integration configuration and the sizes and operating conditions of all pieces of process equipment involved in the integrated process.

The results of the optimal coupling configuration (C1) indicate that a fraction of the steam required in the reboiler of the amine regeneration process of the CO_2 capture plant has to be provided by steam turbines operating at an intermediate pressure level, and the other fraction by two evaporators of the heat recovery steam generators HRSGs. This optimal configuration leads to a minimum mitigation cost –or CO_2 avoided cost– of 90.88 \$/t CO_2 and contributions of the operating and capital expenditures to the total annual cost of 318.18 M \$/yr. and 1870.84 M\$, respectively. The cost associated with fuel consumption is the largest contributor to the operating expenditures with 87.55% (139.56 M\$/yr.), followed by the cooling water with 8.02% (12.79 M\$/yr.), and MEA make-up and inhibitor with 4.36% (6.963 M\$/yr.). On the other hand, 70% of the capital expenditures corresponds to the investments required by the gas turbines (40%), followed by the absorption columns and steam turbines which contribute equally with 15% each. The contribution of compressors is greater than the HRSGs (10 and 8%, respectively), which is also greater than the contribution of the amine regeneration columns (3.20%).

The results of the optimal solution were compared with the results of the suboptimal solutions obtained for the remaining two coupling process configurations studied. When the steam required for the amine regeneration is only extracted from the intermediate/low pressure steam turbine IP/LP ST (configuration C2), the total annual cost is only 0.38% lower than optimal solution (491.58 vs. 493.44 M\$/yr.) but the cost of electric power generation (COE) is 0.70% higher (83.42 vs. 82.84 \$/MWh) implying that the mitigation cost obtained is only 0.15% higher than the optimal coupling configuration (91.02 vs. 90.88 \$/t CO_2). Although both solutions resulted in practically similar mitigation costs, significant differences were observed between them, not only on the operating conditions (flow rate, pressure, and temperature values) but also in the sizes of the heat exchangers in the HRSGs and steam turbines. Thus, the result comparison indicates that it is possible the existence of two different integrated process configurations – with different requirements of total heat transfer area and different levels of electric power generation in the steam turbines – with almost equal mitigation cost. Indeed, the suboptimal configuration which does not include the possibility to directly generate the steam in the HRSG determines a reduction in the total heat transfer area of around 106 dam^2 (1632.40 vs. 1526.41 dam^2) resulting in the generation of 7.92 MW of electric power less than the optimal configuration (744.53 vs. 736.61 MW) but leading to almost equal mitigation cost.

Finally, the optimization results obtained considering that the steam required for the amine regeneration is directly generated in the HRSGs (configuration C3) show a mitigation cost 12.61% higher than the optimal solution (102.34 vs. 90.88 \$/t CO_2) since the cost of electric power generation increased 3.93% (86.10 vs. 82.84 \$/MWh) and the total annual cost value decreased 1.86% (484.24 vs. 493.44 M\$/yr.).

Acknowledgements

The financial support from the Consejo Nacional de Investigaciones Científicas y Técnicas (CONICET) and the Facultad Regional Rosario of the Universidad Tecnológica Nacional from Argentina are gratefully acknowledged.

Appendix A. Supplementary data

Supplementary data associated with this article can be found, in the online version, at http://dx.doi.org/10.1016/j.cej.2017.08.111.

References

[1] R.M. Cuéllar-Franca, A. Azapagic, Carbon capture, storage and utilisation technologies: A critical analysis and comparison of their life cycle environmental impacts, J. CO_2 Util. 9 (2015) 82–102, http://dx.doi.org/10.1016/j.jcou.2014.12.001.

[2] Z. Kravanja, P.S. Varbanov, J.J. Klemeš, Recent advances in green energy and product productions, environmentally friendly, healthier and safer technologies and processes, CO_2 capturing, storage and recycling, and sustainability assessment in decision-making, Clean Techn. Environ. Policy 17 (2015) 1119–1126, http://dx.doi.org/10.1007/s10098-015-0995-9.

[3] T. Blumberg, T. Morosuk, G. Tsatsaronis, Exergy-based evaluation of methanol production from natural gas with CO_2 utilization, Energy (2017), http://dx.doi.org/10.1016/j.energy.2017.06.140.

[4] M. Martín, I.E. Grossmann, Enhanced production of methanol from switchgrass : CO2 to methanol, Proceedings of the 26th European Symposium on Computer Aided Process Engineering – ESCAPE 26. Elsevier B.V., Portorož, Slovenia, (2016) 43–48.

[5] D. Milani, R. Khalilpour, G. Zahedi, A. Abbas, A model-based analysis of CO_2 utilization in methanol synthesis plant, Biochem. Pharmacol. 10 (2015) 12–22, http://dx.doi.org/10.1016/j.jcou.2015.02.003.

[6] K. Roh, R. Frauzem, T.B.H. Nguyen, R. Gani, J.H. Lee, A methodology for the sustainable design and implementation strategy of CO_2 utilization processes, Comp. Chem. Eng. 91 (2016) 407–421, http://dx.doi.org/10.1016/j.compchemeng.2016.01.019.

[7] P. Kongpanna, D.K. Babi, V. Pavarajarn, S. Assabumrungrat, R. Gani, Systematic methods and tools for design of sustainable chemical processes for CO2 utilization, Comp. Chem. Eng. 87 (2016) 125–144, http://dx.doi.org/10.1016/j.compchemeng.2016.01.006.

[8] M. Martín, Optimal year-round production of DME from CO_2 and water using renewable energy, J. CO_2 Util. 13 (2016) 105–113, http://dx.doi.org/10.1016/j.jcou.2016.01.003.

[9] A. Bose, K. Jana, D. Mitra, S. De, Co-production of power and urea from coal with CO_2 capture: performance assessment, Clean Technol. Envir. 17 (5) (2015) 1271–1280, http://dx.doi.org/10.1007/s10098-015-0960-7.

[10] M.M.F. Hasan, E.L. First, F. Boukouvala, C.A. Floudas, A multi-scale framework for CO_2 capture, utilization, and sequestration: CCUS and CCU, Comp. Chem. Eng. 81 (2015) 2–21, http://dx.doi.org/10.1016/j.compchemeng.2015.04.034.

[11] Z. Yuan, M.R. Eden, R. Gani, Toward the development and deployment of large-scale carbon dioxide capture and conversion processes, Ind. Eng. Chem. Res. 55 (12) (2016) 3383–3419, http://dx.doi.org/10.1021/acs.iecr.5b03277.

[12] A.B. Rao, E.S. Rubin, A. Technical, economic, and environmental assessment of amine-based CO_2 capture technology for power plant greenhouse gas control, Environ. Sci. Technol. 36 (2002) 4467–4475, http://dx.doi.org/10.1021/es0158861.

[13] Large-scale CCS facilities | Global carbon capture and storage Institute n.d. https://www.globalccsinstitute.com/projects/large-scale-ccs-projects (accessed August 3, 2017).

[14] R. Idem, T. Supap, H. Shi, D. Gelowitz, M. Ball, C. Campbell, P. Tontiwachwuthikul, Practical experience in post-combustion CO_2 capture using reactive solvents in large pilot and demonstration plants, Int. J. Greenh. Gas Control 40 (2015) 6–25, http://dx.doi.org/10.1016/j.ijggc.2015.06.005.

[15] A. Sánchez-Biezma, J. Paniagua, L. Diaz, M. Lorenzo, J. Alvarez, D. Martínez, B. Arias, M.E. Diego, J.C. Abanades, Testing postcombustion CO2 capture with CaO in a 1.7 MWt pilot facility, Energy Procedia 37 (2013) 1–8, http://dx.doi.org/10.1016/j.egypro.2013.05.078.

[16] T. Stoffregen, S. Rigby, S. Jovanovic, K.R. Krishnamurthy, Pilot-scale demonstration of an advanced aqueous amine-based post-combustion capture technology for CO_2 capture from power plant flue gases, Energy Procedia 63 (2014) 1456–1469, http://dx.doi.org/10.1016/j.egypro.2014.11.155.

[17] M. Akram, U. Ali, T. Best, S. Blakey, K.N. Finney, M. Pourkashanian, Performance evaluation of PACT Pilot-plant for CO_2 capture from gas turbines with exhaust gas recycle, Int. J. Greenh. Gas Control 47 (2016) 137–150, http://dx.doi.org/10.1016/j.ijggc.2016.01.047.

[18] R. Anantharaman, D. Berstad, Energy integration in an NGCC plant with post-combustion CO2 capture – systematic methodology for evaluating process alternatives, Chem. Eng. Trans. 29 (2012) 451–456, http://dx.doi.org/10.3303/CET1229076.

[19] G. Richner, G. Puxty, A. Carnal, W. Conway, M. Maeder, P. Pearson, Thermokinetic properties and performance evaluation of benzylamine-based solvents for CO2 capture, Chem. Eng. J. 264 (2015) 230–240, http://dx.doi.org/10.1016/j.cej.2014.11.067.

[20] K. Fu, W. Rongwong, Z. Liang, Y. Na, R. Idem, P. Tontiwachwuthikul, Experimental analyses of mass transfer and heat transfer of post-combustion CO_2 absorption using hybrid solvent MEA–MeOH in an absorber, Chem. Eng. J. 260 (2015) 11–19, http://dx.doi.org/10.1016/j.cej.2014.08.064.

[21] Y. Du, Y. Wang, G.T. Rochelle, Piperazine/4-Hydroxy-1-methylpiperidine for CO_2 Capture Chem, Eng. J. 307 (2017) 258–263, http://dx.doi.org/10.1016/j.cej.2016.08.095.

[22] S. Loganathan, M. Tikmani, A. Mishra, A.K. Ghoshal, Amine tethered pore-expanded MCM-41 for CO_2 capture: Experimental, isotherm and kinetic modeling studies, Chem. Eng. J. 303 (2016) 89–99, http://dx.doi.org/10.1016/j.cej.2016.05.106.

[23] X. Wang, L. Chen, Q. Guo, Development of hybrid amine-functionalized MCM-41 sorbents for CO_2 capture, Chem. Eng. J. 260 (2015) 573–581, http://dx.doi.org/10.1016/j.cej.2014.08.107.

[24] L. Raynal, P.A. Bouillon, A. Gomez, P. Broutin, From MEA to demixing solvents and future steps, a roadmap for lowering the cost of post-combustion carbon capture, Chem. Eng. J. 171 (3) (2011) 742–752, http://dx.doi.org/10.1016/j.cej.2011.01.008.

[25] Y. Kong, G. Jiang, Y. Wu, S. Cui, X. Shen, Amine hybrid aerogel for high-efficiency CO_2 capture: Effect of amine loading and CO_2 concentration, Chem. Eng. J. 306 (2016) 362–368, http://dx.doi.org/10.1016/j.cej.2016.07.092.

[26] J. Gabrielsen, H.F. Svendsen, M.L. Michelsen, E.H. Stenby, G.M. Kontogeorgis, Experimental validation of a rate-based model for CO_2 capture using an AMP solution, Chem. Eng. Sci. 62 (2007) 2397–2413, http://dx.doi.org/10.1016/j.ces.2007.01.034.

[27] J.D. Figueroa, T. Fout, S. Plasynski, H. McIlvried, R.D. Srivastava, Advances in CO_2 capture technology—The U.S. Department of Energy's Carbon Sequestration Program, Int. J. Greenh. Gas Control 2 (2008) 9–20, http://dx.doi.org/10.1016/S1750-5836(07)00094-1.

[28] K. Li, A. Cousins, H. Yu, P. Feron, M. Tade, W. Luo, J. Chen, Systematic study of aqueous monoethanolamine-based CO_2 capture process: model development and process improvement, Energy Sci. Eng. 4 (1) (2016) 23–39, http://dx.doi.org/10.1002/ese3.101.

[29] A. Veawab, A. Aroonwilas, P. Tontiwachwuthiku, CO_2 absorption performance of aqueous alkanolamines in packed columns, Fuel Chem. Div. P. Repr. 47 (2002) 49–50.

[30] T. Zarogiannis, A.I. Papadopoulos, P. Seferlis, A framework for the preliminary screening of mixtures as post-combustion CO_2 capture solvent candidates, AIChE Annual Meeting, Salt Lake City, (2015).

[31] S. Bommareddy, N.G. Chemmangattuvalappil, C.C. Solvason, M.R. Eden, Simultaneous solution of process and molecular design problems using an algebraic approach, Comput. Chem. Eng. 34 (9) (2010) 1481–1486, http://dx.doi.org/10.1016/j.compchemeng.2010.02.015.

[32] J. Burger, V. Papaioannou, S. Gopinath, G. Jackson, A. Galindo, C.S. Adjiman, A hierarchical method to integrated solvent and process design of physical CO2 absorption using the SAFT-γ Mie approach, AIChE J. 61 (2015) 3249–3269, http://dx.doi.org/10.1002/aic.14838.

[33] A. Chremos, E. Forte, V. Papaioannou, A. Galindo, G. Jackson, C.S. Adjiman, Modelling the phase and chemical equilibria of aqueous solutions of alkanolamines and carbon dioxide using the SAFT-γ SW group contribution approach, Fluid Phase Equilib. 407 (2016) 280–297, http://dx.doi.org/10.1016/j.fluid.2015.07.052.

[34] F.K. Chong, V. Andiappan, D.K.S. Ng, D.C.Y. Foo, F.T. Eljack, M. Atilhan, N.G. Chemmangattuvalappil, Design of ionic liquid as carbon capture solvent for a bioenergy system: integration of bioenergy and carbon capture systems, ACS Sustainable Chem. Eng. 5 (6) (2017) 5241–5252, http://dx.doi.org/10.1021/acssuschemeng.7b00589.

[35] A.I. Papadopoulos, S. Badr, A. Chremos, E. Forte, T. Zarogiannis, P. Seferlis, S. Papadokonstantakis, C.S. Adjiman, A. Galindo, G. Jackson, Efficient screening and selection of post-combustion CO_2 capture solvents, Chem. Eng. Trans. 39 (2014) 211–216, http://dx.doi.org/10.3303/CET1439036.

[36] F. Porcheron, A. Gibert, P. Mougin, A. Wender, High throughput screening of CO_2 solubility in aqueous monoamine solutions, Environ. Sci. Technol. 45 (2011) 2486–2492, http://dx.doi.org/10.1021/es103453f.

[37] M. Stavrou, M. Lampe, A. Bardow, J. Gross, Continuous molecular targeting–computer-aided molecular design (CoMT − CAMD) for simultaneous process and solvent design for CO_2 capture, Ind. Eng. Chem. Res. 53 (2014) 18029–18041, http://dx.doi.org/10.1021/ie502924h.

[38] V. Venkatramana, M. Gupta, M. Foscato, H.F. Svendsen, V.R. Jensen, B.K. Alsberg, Computer-aided molecular design of imidazole-based absorbents for CO_2 capture, Int. J. Greenh. Gas Control 49 (2016) 55–63, http://dx.doi.org/10.1016/j.ijggc.2016.02.023.

[39] M.C. Stern, F. Simeon, H. Herzog, T.A. Hatton, Post-combustion carbon dioxide capture using electrochemically mediated amine regeneration, Energy Environ. Sci. 6 (2013) 2505–2517, http://dx.doi.org/10.1039/C3EE41165F.

[40] M.C. Stern, F. Simeon, H. Herzog, T.A. Hatton, An electrochemically-mediated gas separation process for carbon abatement, Energy Procedia 37 (2013) 1172–1179, http://dx.doi.org/10.1016/j.egypro.2013.05.214.

[41] A.O. Eltayeb, M.C. Stern, H. Herzog, T.A. Hatton, Energetics of electrochemically-mediated amine regeneration, Energy Procedia 63 (2014) 595–604, http://dx.doi.org/10.1016/j.egypro.2014.11.064.

[42] M. Jüdes, S. Vigerske, G. Tsatsaronis, Optimization of the design and partial-load operation of power plants using mixed integer nonlinear programming, Optimization Energy Ind. (2009) 193–220.

[43] E. Martelli, E. Amaldi, S. Consonni, Numerical optimization of heat recovery steam cycles: mathematical model, two-stage algorithm and applications, Comput. Chem. Eng. 35 (2011) 2799–2823, http://dx.doi.org/10.1016/j.compchemeng.2011.04.015.

[44] L. Wang, Y. Yang, C. Dong, T. Morosuk, G. Tsatsaronis, Parametric optimization of supercritical coal-fired power plants by MINLP and differential evolution, Energy Convers. Manag. 85 (2014) 828–838, http://dx.doi.org/10.1016/j.enconman.2014.01.006.

[45] T.M. Tveit, T. Savola, A. Gebremedhin, C.J. Fogelholm, Multi-period MINLP model for optimising operation and structural changes to CHP plants in district heating networks with long-term thermal storage, Energy Convers. Manag. 50 (2009) 639–647, http://dx.doi.org/10.1016/j.enconman.2008.10.010.

[46] J. Zhang, P. Liu, Z. Zhou, L. Ma, Z. Li, W. Ni, A mixed-integer nonlinear programming approach to the optimal design of heat network in a polygeneration energy system, Appl. Energy 114 (2014) 146–154, http://dx.doi.org/10.1016/j.apenergy.2013.09.057.

[47] J.I. Manassaldi, A.M. Arias, N.J. Scenna, M.C. Mussati, S.F. Mussati, A discrete and continuous mathematical model for the optimal synthesis and design of dual pressure heat recovery steam generators coupled into two steam turbines, Energy 103 (2016) 807–823, http://dx.doi.org/10.1016/j.energy.2016.02.129.

[48] I. Nowak, H. Alperin, S. Vigerske, LaGO – An object oriented library for solving MINLPs. Global optimization and constraint satisfaction, Ser. Lecture Notes Comput. Sci. 2861 (2003) 32–42.

[49] J.Y. Kang, D.W. Kang, T.S. Kim, K.B. Hur, Economic evaluation of biogas and natural gas co-firing in gas turbine combined heat and power systems, Appl. Thermal Eng. 70 (2014) 723–731, http://dx.doi.org/10.1016/j.applthermaleng.2014.05.085.

[50] D.W. Kang, T.S. Kim, K.B. Hur, J.K. Park, The effect of firing biogas on the performance and operating characteristics of simple and recuperative cycle gas turbine combined heat and power systems, Appl. Energy 93 (2012) 215–228, http://dx.doi.org/10.1016/j.apenergy.2011.12.038.

[51] E. León, M. Martín, Optimal production of power in a combined cycle from manure based biogas, Energy Convers. Manag. 114 (2016) 89–99, http://dx.doi.org/10.1016/j.enconman.2016.02.002.

[52] H. Yağlı, Y. Koç, A. Koç, A. Görgülü, A. Tandiroğlu, Parametric optimization and exergetic analysis comparison of subcritical and supercritical organic Rankine cycle (ORC) for biogas fuelled combined heat and power (CHP) engine exhaust gas waste heat, Energy 111 (2016) 923–932, http://dx.doi.org/10.1016/j.energy.2016.05.119.

[53] GateCycle Software Alternatives and Similar Software - AlternativeTo.net. AlternativeTo n.d. http://alternativeto.net/software/gatecycle-software/ (accessed August 2, 2017).

[54] S.E. Hosseini, M.A. Wahid, Developments of biogas combustion in combined heat and power generation, Renew. Sust. Energy Rev. 40 (2014) 868–875, http://dx.doi.org/10.1016/j.rser.2014.07.204.

[55] M. Zhang, Y. Guo, Reaction sensitivity analysis of regeneration process of CO_2 capture using aqueous ammonia, Chem. Eng. J. 272 (2015) 135–144, http://dx.doi.org/10.1016/j.cej.2015.03.030.

[56] H. Thee, Y.A. Suryaputradinata, K.A. Mumford, K.H. Smith, G. da Silva, S.E. Kentish, G.W. Stevens, A kinetic and process modeling study of CO2 capture with MEA-promoted potassium carbonate solutions, Chem. Eng. J. 210 (2012) 271–279, http://dx.doi.org/10.1016/j.cej.2012.08.092.

[57] Y.J. Lin, G.T. Rochelle, Approaching a reversible stripping process for CO_2 capture, Chem. Eng. J. 283 (2016) 1033–1043, http://dx.doi.org/10.1016/j.cej.2015.08.086.

[58] L. Peters, A. Hussain, M. Follmann, T. Melin, M.B. Hägg, CO_2 removal from natural gas by employing amine absorption and membrane technology—A technical and economic analysis, Chem. Eng. J. 172 (2–3) (2011) 952–960, http://dx.doi.org/10.1016/j.cej.2011.07.007.

[59] U. Lee, A. Mitsos, C. Han, Optimal retrofit of a CO_2 capture pilot plant using superstructure and rate-based models, Int. J. Greenh. Gas Control 50 (2016) 57–69, http://dx.doi.org/10.1016/j.ijggc.2016.03.024.

[60] N. Rodríguez, S.F. Mussati, N.J. Scenna, Optimization of post-combustion CO_2 process using DEA–MDEA mixtures, Chem. Eng. Res. Des. 89 (9) (2011) 1763–1773, http://dx.doi.org/10.1016/j.cherd.2010.11.009.

[61] Z.H. Liang, T. Sanpasertparnich, P. Tontiwachwuthikul, D. Gelowitz, R. Idem, Part 1: Design, modeling and simulation of post-combustion CO_2 capture systems using reactive solvents, Carbon Manag. 2 (3) (2011) 265–288, http://dx.doi.org/10.

4155/cmt.11.19.
[62] J. Gáspár, A.M. Cormoş, Dynamic modeling and validation of absorber and desorber columns for post-combustion CO_2 capture, Comput. Chem. Eng. 35 (2011) 2044–2052, http://dx.doi.org/10.1016/j.compchemeng.2010.10.001.
[63] J.A. Wurzbacher, C. Gebald, S. Brunner, A. Steinfeld, Heat and mass transfer of temperature–vacuum swing desorption for CO_2 capture from air, Chem. Eng. J. 283 (2016) 1329–1338, http://dx.doi.org/10.1016/j.cej.2015.08.035.
[64] T. Sema, A. Naami, K. Fu, M. Edali, H. Liu, H. Shi, Z. Liang, R. Idem, P. Tontiwachwuthikul, Comprehensive mass transfer and reaction kinetics studies of CO_2 absorption into aqueous solutions of blended MDEA–MEA, Chem. Eng. J. 209 (2012) 501–512, http://dx.doi.org/10.1016/j.cej.2012.08.016.
[65] A. Lawal, M. Wang, P. Stephenson, H. Yeung, Dynamic modelling of CO_2 absorption for post combustion capture in coal-fired power plants, Fuel 88 (2009) 2455–2462, http://dx.doi.org/10.1016/j.fuel.2008.11.009.
[66] A. Alhajaj, N. MacDowell, N. Shah, Multiscale design and analysis of CO_2 capture, Transp. Storage Netw. Energy Procedia 37 (2013) 2552–2561, http://dx.doi.org/10.1016/j.egypro.2013.06.138.
[67] A. Alhajaj, N. Mac Dowell, N. Shah, A techno-economic analysis of post-combustion CO2 capture and compression applied to a combined cycle gas turbine: Part II. Identifying the cost-optimal control and design variables, Int. J. Greenh. Gas Control 52 (2016) 331–343, http://dx.doi.org/10.1016/j.ijggc.2016.07.008.
[68] N. Mac Dowell, N. Shah, Dynamic modelling and analysis of a coal-fired power plant integrated with a novel split-flow configuration post-combustion CO_2 capture process, Int. J. Greenh. Gas Control 27 (2014) 103–119, http://dx.doi.org/10.1016/j.ijggc.2014.05.007.
[69] J. Rodriguez, A. Andrade, A. Lawal, N. Samsatli, M. Calado, A. Ramos, T. Lafitte, J. Fuentes, C.C. Pantelides, An integrated framework for the dynamic modelling of solvent based CO_2 capture processes, Energy Procedia 63 (2014) 1206–1217, http://dx.doi.org/10.1016/j.egypro.2014.11.130.
[70] N. Harun, P.L. Douglas, L. Ricardez-Sandoval, E. Croiset, Dynamic simulation of MEA absorption processes for CO2 capture from fossil fuel power plant, Energy Procedia 4 (2011) 1478–1485, http://dx.doi.org/10.1016/j.egypro.2011.02.014.
[71] N. Ceccarelli, M. van Leeuwen, T. Wolf, P. van Leeuwen, R. van der Vaart, W. Maas, A. Ramos, Flexibility of low-CO_2 gas power plants: Integration of the CO2 capture unit with CCGT operation, Energy Procedia 63 (2014) 1703–1726, http://dx.doi.org/10.1016/j.egypro.2014.11.179.
[72] H.M. Kvamsdal, G.T. Rochelle, Effects of the temperature bulge in CO_2 absorption from flue gas by aqueous monoethanolamine, Ind. Eng. Chem. Res. 47 (3) (2008) 867–875, http://dx.doi.org/10.1021/ie061651s.
[73] H.M. Kvamsdal, J.P. Jakobsen, K.A. Hoff, Dynamic modeling and simulation of a CO_2 absorber column for post-combustion CO_2 capture, Chem. Eng. Process. 48 (2009) 135–144, http://dx.doi.org/10.1016/j.cep.2008.03.002.
[74] M.S. Walters, T.F. Edgar, G.T. Rochelle, Dynamic modeling and control of an intercooled absorber for post-combustion CO_2 capture, Chem. Eng. Process. 107 (2016) 1–10, http://dx.doi.org/10.1016/j.cep.2016.05.012.
[75] M.T. Luu, N. Abdul Manaf, A. Abbas, Dynamic modelling and control strategies for flexible operation of amine-based post-combustion CO_2 capture systems, Int. J. Greenh. Gas Control 39 (2015) 377–389, http://dx.doi.org/10.1016/j.ijggc.2015.05.007.
[76] J.H. Meldon, M.A. Morales-Cabrera, Analysis of carbon dioxide absorption in and stripping from aqueous monoethanolamine, Chem. Eng. J. 171 (3) (2011) 753–759, http://dx.doi.org/10.1016/j.cej.2011.05.099.
[77] S. Freguia, G.T. Rochelle, Modeling of CO_2 Capture by aqueous monoethanolamine, AIChE J. 49 (2003) 1676–1686, http://dx.doi.org/10.1002/aic.690490708.
[78] P.L. Mores, N.J. Scenna, S.F. Mussati, Post-combustion CO_2 capture process: equilibrium stage mathematical model of the chemical absorption of CO_2 into Monoethanolamine (MEA) aqueous solution, Chem. Eng. Res. Des. 89 (9) (2011) 1587–1599, http://dx.doi.org/10.1016/j.cherd.2010.10.012.
[79] P.L. Mores, N. Rodríguez, N.J. Scenna, S.F. Mussati, CO_2 capture in power plants: minimization of the investment and operating cost of the post-combustion process using MEA aqueous solution, Int. J. Greenh. Gas Control 10 (2012) 148–163, http://dx.doi.org/10.1016/j.ijggc.2012.06.002.
[80] P.L. Mores, N.J. Scenna, S.F. Mussati, CO_2 capture using Monoethanolamine (MEA) aqueous solution: modeling and optimization of the solvent regeneration and CO_2 desorption process, Energy 45 (2012) 1042–1058, http://dx.doi.org/10.1016/j.energy.2012.06.038.
[81] P.L. Mores, N.J. Scenna, S.F. Mussati, A rate based model of a packed column for CO_2 absorption using aqueous monoethanolamine solution, Int. J. Greenh. Gas Control 6 (2012) 21–36, http://dx.doi.org/10.1016/j.ijggc.2011.10.012.
[82] T. Damartzis, A.I. Papadopoulos, P. Seferlis, Process flowsheet design optimization for various amine-based solvents in post-combustion CO_2 capture plants, J. Clean. Prod. 111 (Part A) (2016) 204–216, http://dx.doi.org/10.1016/j.jclepro.2015.04.129.
[83] A.M. Arias, P.L. Mores, N.J. Scenna, S.F. Mussati, Optimal design and sensitivity analysis of post-combustion CO_2 capture process by chemical absorption with amines, J. Clean. Prod. 115 (2016) 315–331, http://dx.doi.org/10.1016/j.jclepro.2015.12.056.
[84] T. Adams, N. Mac Dowell, Off-design point modelling of a 420 MW CCGT power plant integrated with an amine-based post-combustion CO2 capture and compression process, Appl. Energy 178 (2016) 681–702, http://dx.doi.org/10.1016/j.apenergy.2016.06.087.
[85] U. Ali, C. Font-Palmab, M. Akrama, E.O. Agbonghaec, Comparative potential of natural gas, coal and biomass fired power plant with post-combustion CO_2 capture and compression, Int. J. Greenh. Gas Control 63 (2017) 184–193, http://dx.doi.org/10.1016/j.ijggc.2017.05.022.
[86] R.M. Montañés, S.O. Gar Darsdóttir, F. Normann, F. Johnsson, L.O. Nord, Demonstrating load-change transient performance of a commercial-scale natural gas combined cycle power plant with post-combustion CO_2 capture, Int. J. Greenh. Gas Control 63 (2017) 158–174, http://dx.doi.org/10.1016/j.ijggc.2017.05.011.
[87] P. Tait, B. Buschle, I. Ausner, P. Valluri, M. Wehrli, M. Lucquiaud, A pilot-scale study of dynamic response scenarios for the flexible operation of post-combustion CO_2 capture, Int. J. Greenh. Gas Control 48 (2016) 216–233, http://dx.doi.org/10.1016/j.ijggc.2015.12.009.
[88] M.S. Walters, Y.J. Lin, D.J. Sachde, T.F. Edgar, G.T. Rochelle, Control relevant model of amine scrubbing for CO_2 capture from power plants, Ind. Eng. Chem. Res. 55 (2016) 1690–1700, http://dx.doi.org/10.1021/acs.iecr.5b04379.
[89] Combined Cycle - THERMOFLEX n.d. https://www.thermoflow.com/combinedcycle_TFX.html (accessed August 19, 2017).
[90] N. Dave, T. Do, D. Palfreyman, P.H.M. Feron, Impact of liquid absorption process development on the costs of post-combustion capture in Australia coal-fired power stations, Chem. Eng. Res. Des 89 (2011) 1625–1638, http://dx.doi.org/10.1016/j.cherd.2010.09.010.
[91] R. Carapellucci, L. Giordano, M. Vaccarelli, Studying heat integration options for steam-gas power plants retrofitted with CO_2 post-combustion capture, Energy 85 (2015) 594–608, http://dx.doi.org/10.1016/j.energy.2015.03.071.
[92] J. Gibbins, H. Chalmers, M. Lucquiaud, J. Li, N. McGlashan, X. Liang, J. Davison, Techno-economic assessment of CO_2 capture retrofit to existing power plants, Energy Procedia 4 (2011) 1835–1842, http://dx.doi.org/10.1016/j.egypro.2011.02.061.
[93] X. Liang, J. Li, Assessing the value of retrofitting cement plants for carbon capture: a case study of a cement plant in Guangdong, China, Energy Convers. Manag. 64 (2012) 454–465, http://dx.doi.org/10.1016/j.enconman.2012.04.012.
[94] M. Sanchez del Rio, M. Lucquiaud, J. Gibbins, Maintaining the power output of an existing coal plant with the addition of CO_2 capture: retrofits options with gas turbine combined cycle plants, Energy Procedia 63 (2014) 2530–2541, http://dx.doi.org/10.1016/j.egypro.2014.11.275.
[95] A. Aboudheir, W. Elmoudir, Optimization of an existing 130 Tonne Per Day CO_2 capture plant from a flue gas slip stream of a coal power plant, Energy Procedia 37 (2013) 1509–1516, http://dx.doi.org/10.1016/j.egypro.2013.06.026.
[96] G. Xu, Y. Yang, J. Ding, S. Li, W. Liu, K. Zhang, Analysis and optimization of CO_2 capture in an existing coal-fired power plant in China, Energy 58 (2013) 117–127, http://dx.doi.org/10.1016/j.energy.2013.04.012.
[97] J. Li, X. Liang, CO_2 capture modeling for pulverized coal-fired power plants: a case study of an existing 1 GW ultra-supercritical power plant in Shandong, China, Sep. Purif. Technol. 94 (2012) 138–145, http://dx.doi.org/10.1016/j.seppur.2011.09.044.
[98] D. Singh, E. Croiset, P.L. Douglas, M.A. Douglas, Techno-economic study of CO_2 capture from an existing coal-fired power plant: MEA scrubbing vs. O_2/CO_2 recycle combustion, Energy Convers. Manag. 44 (19) (2003) 3073–3091, http://dx.doi.org/10.1016/S0196-8904(03)00040-2.
[99] M. Pan, F. Aziz, B. Li, S. Perry, N. Zhang, I. Bulatov, R. Smith, Application of optimal design methodologies in retrofitting natural gas combined cycle power plants with CO_2 capture, Appl. Energy 161 (2016) 695–706, http://dx.doi.org/10.1016/j.apenergy.2015.03.035.
[100] D.P. Hanak, C. Biliyok, V. Manovic, Efficiency improvements for the coal-fired power plant retrofit with CO_2 capture plant using chilled ammonia process, Appl. Energy 151 (2015) 258–272, http://dx.doi.org/10.1016/j.apenergy.2015.04.059.
[101] D.H. Van Wagener, U. Liebenthal, J.M. Plaza, A. Kather, G.T. Rochelle, Maximizing coal-fired power plant efficiency with integration of amine-based CO_2 capture in greenfield and retrofit scenarios, Energy 72 (2014) 824–831, http://dx.doi.org/10.1016/j.energy.2014.04.117.
[102] J.I. Manassaldi, P.L. Mores, N.J. Scenna, S.F. Mussati, Optimal design and operating conditions of an integrated plant using a natural gas combined cycle and post-combustion CO_2 capture, Ind. Eng. Chem. Res. 53 (44) (2014) 17026–17042, http://dx.doi.org/10.1021/ie5004637.
[103] P.L. Mores, E. Godoy, S.F. Mussati, N.J. Scenna, A NGCC power plant with a CO_2 post-combustion capture option, optimal economics for different generation/capture goals, Chem. Eng. Res. Des. 92 (7) (2014) 1329–1353, http://dx.doi.org/10.1016/j.cherd.2013.11.013.
[104] J. Wang, Z. Sun, Y. Dai, S. Ma, Parametric optimization design for supercritical CO_2 power cycle using genetic algorithm and artificial neural network, Appl. Energy 87 (4) (2010) 1317–1324, http://dx.doi.org/10.1016/j.apenergy.2009.07.017.
[105] H. Li, F. Maréchal, M. Burer, D. Favrat, Multi-objective optimization of an advanced combined cycle power plant including CO_2 separation options, Energy 31 (15) (2006) 3117–3134, http://dx.doi.org/10.1016/j.energy.2006.03.014.
[106] L. Tock, F. Maréchal, Environomic optimal design of power plants with CO_2 capture, Int. J. Greenh. Gas Control 39 (2015) 245–255, http://dx.doi.org/10.1016/j.ijggc.2015.05.022.
[107] J. Cristóbal, G. Guillén-Gosálbez, L. Jiménez, A. Irabien, Multi-objective optimization of coal-fired electricity production with CO_2 capture, Applied Energy 98 (2012) 266–272, http://dx.doi.org/10.1016/j.apenergy.2012.03.036.
[108] I. Kantor, A. Betancourt, A. Elkamel, M. Fowler, A. Almansoori, Generalized mixed-integer nonlinear programming modeling of eco-industrial networks to reduce cost and emissions, J. Clean. Prod. 99 (15) (2015) 160–176, http://dx.doi.org/10.1016/j.jclepro.2015.03.017.
[109] J. Cristóbal, G. Guillén-Gosálbez, A. Kraslawski, A. Irabien, Stochastic MILP model for optimal timing of investments in CO_2 capture technologies under uncertainty in prices, Energy 54 (2013) 343–351, http://dx.doi.org/10.1016/j.energy.2013.01.068.
[110] O. Akgul, N. Mac Dowell, L.G. Papageorgiou, N. Shah, A mixed integer nonlinear

programming (MINLP) supply chain optimisation framework for carbon negative electricity generation using biomass to energy with CCS (BECCS) in the UK, Int. J. Greenh. Gas Control 28 (2014) 189–202, http://dx.doi.org/10.1016/j.ijggc.2014.06.017.
[111] E. Martelli, L.O. Nord, O. Bolland, Design criteria and optimization of heat recovery steam cycles for integrated reforming combined cycles with CO_2 capture, Appl. Energy 92 (2012) 255–268, http://dx.doi.org/10.1016/j.apenergy.2011.10.043.
[112] J.C. Eslick, D.C. Miller, A multi-objective analysis for the retrofit of a pulverized coal power plant with a CO_2 capture and compression process, Comput. Chem. Eng. 35 (2011) 1488–1500, http://dx.doi.org/10.1016/j.compchemeng.2011.03.020.
[113] P. Feron, Absorption-Based Post-Combustion Capture of Carbon Dioxide, Woodhead Publishing Series in Energy, UK, 2016.
[114] A. González-Díaz, A.M. Alcaráz-Calderón, M.O. González-Díaz, A. Méndez-Aranda, M. Lucquiaud, J.M. González-Santaló, Effect of the ambient conditions on gas turbine combined cycle power plants with post-combustion CO_2 capture, Energy 134 (1) (2017) 221–233, http://dx.doi.org/10.1016/j.energy.2017.05.020.
[115] G.T. Rochelle, Amine scrubbing for CO_2 capture, Science 325 (2009) 1652–1654, http://dx.doi.org/10.1126/science.1176731.
[116] L.E. Øi, J. Lundberg, M. Pedersen, P.M. Hansen, M.C. Melaaen, Laboratory Rig for atmospheric CO_2 absorption and desorption under pressure, Energy Procedia 37 (2013) 1933–1940, http://dx.doi.org/10.1016/j.egypro.2013.06.074.
[117] E.R. Dugas, Pilot Plant Study of Carbon Dioxide Capture by Aqueous Ethanolamine, M.S.E. Thesis University of Texas at Austin, 2006.
[118] P. Tontiwachwuthikul, A. Meisen, C.J. Lim, CO_2 absorption by NaOH, monoethanolamine, and 2-amino-2-methyl-1-propanol solutions in a packed column, Chem. Eng. Sci. 47 (1992) 381–390, http://dx.doi.org/10.1016/0009-2509(92)80028-B.
[119] I. Alatiqi, M. Fk, W. Sabri, E. Alper Bouhamra, Steady-state rate-based modelling for CO_2/amine absorption–desorption systems, Gas Sep. Purif. 8 (1994) 3–11, http://dx.doi.org/10.1016/0950-4214(94)85002-X.
[120] D.M. Austgen, A model of vapor-liquid equilibria for acid gas-alkanolamine-water systems, Ph.D. thesis University of Texas at Austin, 1989.
[121] B.A. Oyenekan, G.T. Rochelle, Alternative stripper configurations for CO_2 capture by aqueous amines, AIChE J. 53 (2007) 3144–3154, http://dx.doi.org/10.1002/aic.11316.
[122] M.D. Hilliard, A Predictive Thermodynamic Model for an Aqueous Blend of Potassium Carbonate, Piperazine, and Monoethanolamine for Carbon Dioxide Capture from Flue Gas, PhD Thesis University of Texas at Austin, Austin, TX, 2008.
[123] A. Aboudheir, P. Tontiwachwuthikul, A. Chakma, R. Idem, Kinetics of the reactive absorption of carbon dioxide in high CO_2-loaded, concentrated aqueous monoethanolamine solutions, Chem. Eng. Sci. 58 (2003) 5195–5210, http://dx.doi.org/10.1016/j.ces.2003.08.014.
[124] Y. Liu, L. Zhang, S. Watanasiri, Representing vapor-liquid equilibrium for an aqueous MEA-CO_2 system using the electrolyte nonrandom-two-liquid model, Ind. Eng. Chem. Res. 38 (1999) 2080–2090, http://dx.doi.org/10.1021/ie980600v.
[125] T. Greer, Modeling and simulation of post combustion CO_2 capturing, Master Thesis Telemark University College, Faculty of Technlogy, Porsgrunn, Norway, 2008.
[126] M. Leva, Reconsider packed-tower pressure-drop correlations, Chem. Eng. Prog. A 88 (1992) 65–72.
[127] W.D. Seider, J.D. Seader, D.R. Lewin, S. Widagdo, Product and Process Design Principles: Synthesis, Analysis and Design, John Wiley and Sons, USA, 2009.
[128] D. Chapel, J. Ernest, C. Mariz, Recovery of CO2 from flue gases: commercial trends, Canadian Society of Chemical Engineers annual meeting, October 4-6, 1999, Saskatoon, Saskatchewan, Canada.
[129] K. Onda, H. Takeuchi, Y. Okumoto, Mass transfer coefficients between gas and liquid phases in packed columns, J. Chem. Eng. Jpn. 1 (1) (1968) 56–62.
[130] L. Kucka, E.Y. Kenig, A. Górak, Kinetics of the gas–liquid reaction between carbon dioxide and hydroxide ions, Ind. Eng. Chem. Res. 41 (2002) 5952–5957, http://dx.doi.org/10.1021/ie020452f.
[131] L.A. Robbins, Improve pressure-drop prediction with a new correlation, Chem. Eng. Prog. 87 (1991) 87–90.
[132] H. Kister, Distillation Design, 1st ed., McGraw-Hill Education, New York, USA, 1992.
[133] R.C. Reid, The Properties of Gases and Liquids, McGraw-Hill, USA, 1987.
[134] H.A. Al-Ghawas, D.P. Hagewiesche, G. Ruiz-Ibanez, O.C. Sandall, O.C., Physicochemical properties important for carbon dioxide absorption in aqueous methyldiethanolamine, J. Chem. Eng. Data 34 (1989) 385–391, http://dx.doi.org/10.1021/je00058a004.
[135] G.F. Versteeg, W. Van Swaalj, Solubility and diffusivity of acid gases (carbon dioxide, nitrous oxide) in aqueous alkanolamine solutions, J. Chem. Eng. Data 33 (1988) 29–34, http://dx.doi.org/10.1021/je00051a011.
[136] R. Maceiras, E. Álvarez, M.A. Cancela, Effect of temperature on carbon dioxide absorption in monoethanolamine solutions, Chem. Eng. J. 138 (2008) 295–300, http://dx.doi.org/10.1016/j.cej.2007.05.049.
[137] H. Li, F. Marechal, D. Favrat, Power and cogeneration technology environomic performance typification in the context of CO2 abatement part I: Power generation, Energy 35 (2010) 3143–3154, http://dx.doi.org/10.1016/j.energy.2010.03.004.
[138] B.E. Poling, J.M. Prausnitz, J.P. O'Connell, The Properties of Gases and Liquids, McGraw-Hill Education, 2000 768 p.
[139] W. Wagner, H.J. Kretzschmar, International Steam Tables – Properties of Water and Steam based on the Industrial Formulation IAPWS-IF97, Springer Science & Business Media, Netherlands, 2007.
[140] M.R.M. Abu-Zahra, J.P.M. Niederer, P.H.M. Feron, D.F. Versteeg, CO_2 capture from power plants: Part II. A parametric study of the economic performance based on mono-ethanolamine, Int. J. Greenh. Gas Control 1 (2007) 135–142, http://dx.doi.org/10.1016/S1750-5836(07)00032-1.
[141] A.B. Rao, E.S. Rubin, A. Technical, Economic, and environmental assessment of amine-based CO_2 capture technology for power plant greenh. gas control, Environ. Sci. Technol. 36 (2002) 4467–4475, http://dx.doi.org/10.1021/es0158861.
[142] A.B. Rao, E.S. Rubin, Identifying cost-effective CO_2 control levels for amine-based CO_2 capture systems, Ind. Eng. Chem. Res. 45 (2006) 2421–2429, http://dx.doi.org/10.1021/ie050603p.
[143] G. Ferrara, A. Lanzini, P. Leone, M.T. Ho, D.E. Wiley, Exergetic and exergoeconomic analysis of post-combustion CO_2 capture using MEA-solvent chemical absorption, Energy 130 (2017) 113–128, http://dx.doi.org/10.1016/j.energy.2017.04.096.
[144] C. Henao, Simulación y evaluación de procesos químicos, Herramientas básicas para la síntesis de procesos, Universidad Pontificia Bolivariana, Medellín, Colombia, 2010.
[145] Matches' 275 Equipment Cost Estimates. n.d. http://www.matche.com/equipcost/Default.html (accessed June 22, 2017).
[146] D. McCollum, J. Ogden, Techno-Economic Models for Carbon Dioxide Compression, Transport, and Storage & Correlations for Estimating Carbon Dioxide Density and Viscosity, Institute of Transportation Studies, University of California, California, USA, 2006.
[147] Nye Thermodynamics Corporation, 2013. Gas Turbine Prices. http://www.gas-turbines.com. (accessed, 2013).
[148] U.S. Energy Information Administration, Updated capital cost estimates for electricity generation plants. U.S. Department of Energy, Washington DC, USA, 2010.
[149] E. Mayer, Chemical Engineering Plant Cost CEPCI 2014, 2016.
[150] K.S. Fisher, C. Beitler, C. Rueter, K. Searcy, G. Rochelle, M. Jassim, J. Figueroa, Integrating MEA regeneration with CO_2 compression to reduce CO_2 capture costs, Fourth Annual Conference on Carbon Capture and Sequestration DOE/NETL (2005) May 2–5, 2005, (2005).
[151] U.S. Department of Energy, 2013. U.S. Energy Information Administration. http://www.eia.gov.
[152] G. Ulrich, P. Vasudevan, How to estimate utility costs, Chem. Eng. 119 (2010) 66–69.
[153] A. Drud, CONOPT: a GRG code for large sparse dynamic nonlinear optimization problems, Math. Program. 31 (2) (1985) 153–191.